CHARACTERIZATION OF FROTHERS BY WATER CARRYING RATE

Pamela Moyo

Department of Mining, Metals and Materials Engineering
McGill University
Montreal, Canada

April 2005

A thesis submitted to the Faculty of Graduate Studies and Research
in partial fulfillment of the requirements of the degree of
Master of Engineering

© Pamela Moyo, 2005

Library and
Archives Canada

Published Heritage
Branch

395 Wellington Street
Ottawa ON K1A 0N4
Canada

Bibliothèque et
Archives Canada

Direction du
Patrimoine de l'édition

395, rue Wellington
Ottawa ON K1A 0N4
Canada

Your file Votre référence
ISBN: 978-0-494-22658-2
Our file Notre référence
ISBN: 978-0-494-22658-2

NOTICE:
The author has granted a non-exclusive license allowing Library and Archives Canada to reproduce, publish, archive, preserve, conserve, communicate to the public by telecommunication or on the Internet, loan, distribute and sell theses worldwide, for commercial or non-commercial purposes, in microform, paper, electronic and/or any other formats.

The author retains copyright ownership and moral rights in this thesis. Neither the thesis nor substantial extracts from it may be printed or otherwise reproduced without the author's permission.

AVIS:
L'auteur a accordé une licence non exclusive permettant à la Bibliothèque et Archives Canada de reproduire, publier, archiver, sauvegarder, conserver, transmettre au public par télécommunication ou par l'Internet, prêter, distribuer et vendre des thèses partout dans le monde, à des fins commerciales ou autres, sur support microforme, papier, électronique et/ou autres formats.

L'auteur conserve la propriété du droit d'auteur et des droits moraux qui protège cette thèse. Ni la thèse ni des extraits substantiels de celle-ci ne doivent être imprimés ou autrement reproduits sans son autorisation.

In compliance with the Canadian Privacy Act some supporting forms may have been removed from this thesis.

While these forms may be included in the document page count, their removal does not represent any loss of content from the thesis.

Conformément à la loi canadienne sur la protection de la vie privée, quelques formulaires secondaires ont été enlevés de cette thèse.

Bien que ces formulaires aient inclus dans la pagination, il n'y aura aucun contenu manquant.

Canada

ABSTRACT

In flotation, bubbles are the transport medium of mineral particles and water. The recovery of fine hydrophilic gangue is related to the recovery of water, which impacts the grade of the concentrate. In the solution (pulp) phase, water is transported as a layer on the bubble surface and as a trailing wake. The amount of water depends on bubble size, gas rate and, it is hypothesized, frother type.

Frothers are surface-active reagents that reduce bubble size by retarding coalescence. To isolate the effect of frother type (chemistry) on water transport from that of bubble size and gas rate an appropriate independent variable had to be established. Bubble surface area flux and gas holdup were proposed and correlated against the overflow rate of water from a bubble column at a given foam depth which was used as a measure of water carrying rate.

Gas holdup is established as the independent variable and it is shown that the common frothers can be grouped into families based on the gas holdup-carrying rate relationship. No relation was found between water carrying rate and bubble surface area flux. Possible reasons are considered.

RESUME

Dans le procédé de flottation, les bulles constituent le médium de transport pour l'eau et les particules de minerais. La récupération des particules hydrophiles fines de gangue est reliée à la récupération d'eau, influençant ainsi la teneur du concentré. Dans la phase soluble (pulpe), l'eau est transportée sous forme de couche à la surface des bulles ainsi que dans le sillage de celles-ci.

Les moussants sont des surfactants qui réduisent la grosseur des bulles en retardant la coalescence. Afin d'isoler l'effet du type de moussant (chimie) sur le transport d'eau de la grosseur des bulles et du débit de gaz, une variable indépendante appropriée a du être choisie. Le flux d'aire de surface des bulles et la rétention de gaz ont été proposés et corrélés contre la vitesse de déversement d'eau d'une colonne à bulles à une hauteur d'écume donnée, utilisée comme mesure de vitesse de transport d'eau.

La rétention de gaz est établie comme la variable indépendante et il est démontré que les moussants communs peuvent être regroupés en familles basé sur la relation rétention de gaz-vitesse de transport. Aucun lien ne semble exister entre la vitesse de transport d'eau et le flux d'aire de surface des bulles. Les raisons possibles de cette observation sont considérées.

ACKNOWLEDGEMENTS

I would like to thank Prof. Finch for his guidance, encouragement and kindness during the course of this work. I would also like to thank Dr. Gomez for all his efforts in giving me direction and attainment of the equipment used in this project.

To the Jim Finch group (old and new) I say thank you for making me smile and providing support and encouragement during the smooth and rough rides of my work. You made my time at McGill worthwhile and I learned a lot from all of you.

Lastly, but not least, to my family, Bongani ngiyabonga for giving me all the support I needed particularly those days. Thandiwe, ngiyakuthanda mntanami, you gave me all the happiness I needed in my life.

TABLE OF CONTENTS

LIST OF FIGURES

LIST OF TABLES

CHAPTER 1

INTRODUCTION

1.1 GENERAL BACKGROUND

Mineral processing involves two principal operations: size reduction to liberate minerals and separation of valuable minerals from the gangue. The extent of size reduction depends on the distribution of valuable mineral grains in the ore matrix; the finer the grain size the greater the size reduction needed. Size reduction or comminution is conducted in stages from coarse crushing (e.g., 1.5m to 10cm) to fine grinding (increasingly < 25μm) where the target degree of liberation is achieved [Wills, 1997].

Communition is the "feed preparation" step readying the minerals for separation. The most versatile technique used to separate finely divided solid particles is flotation. Flotation utilizes the difference in surface chemistry (wettability) of minerals in water, floating hydrophobic minerals and rejecting hydrophilic ones. The ground ore particles are mixed with water to form a slurry, typically 20-30% by weight. While some minerals are naturally hydrophobic like coal (considered a mineral for discussion purposes), most minerals are hydrophilic and are rendered hydrophobic by addition of reagents called collectors.

Flotation is carried out in machines where bubbles are generated and dispersed by passing air through a rotating impeller in the case of mechanical machines, various spargers in the case of flotation columns and self-aspiration through an orifice in the case of Jameson cells. The process has two distinct zones (Figure 1.1):

(a) Collection (or pulp) zone

Here bubbles are generated and dispersed in the slurry where bubble-particle collision and attachment takes place. Hydrophobic particles attach to the bubble leaving the hydrophilic ones in the pulp. The resulting bubble-particle aggregates rise to the surface of the slurry where they accumulate to form the froth zone. The hydrophilic particles in the pulp exit the cell as tails.

(b) Froth zone

In the froth zone, three processes can be identified:

(i) bubble-particle aggregates are transported over the flotation cell lip and collected (vertical bubble motion is transferred to horizontal);

(ii) loosely attached particles detach (i.e., less hydrophobic ones) from the bubble;

(iii) particles entrained in water drain back to the collection zone.

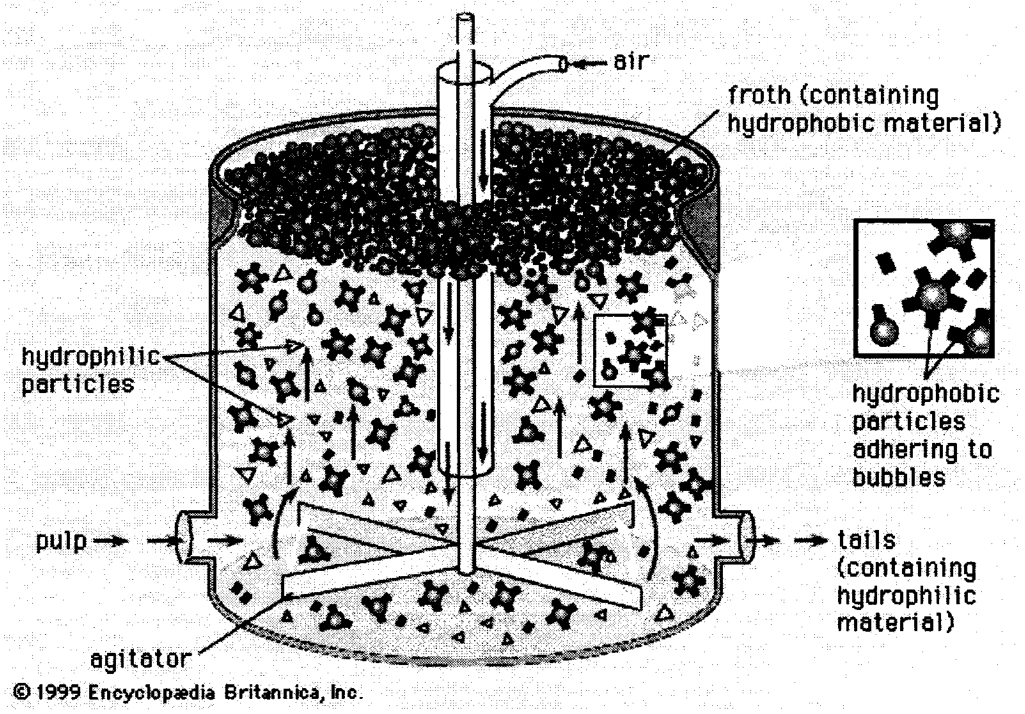

© 1999 Encyclopædia Britannica, Inc.

FIGURE 1.1: *Schematic of a mechanical flotation machine indicating the two zones, pulp and froth [Encyclopaedia Britannica, 1999]*

Bubbles not only transport particles but also transport water. In the collection zone, water is carried both as a layer on the bubble surface and as a trailing wake (Figure 1.2). To increase particle recovery rates, the target is to produce a high population of small bubbles to give high surface area to volume ratio. This will also increase the amount of water transported. Thus whatever action is taken to decrease the size and increase the number of bubbles to increase particle recovery rate will concomitantly tend to increase the recovery rate of water. Since water entrains particles unselectively, the amount of water recovered to the overflow has a major impact on the recovery of gangue and thus the grade of the concentrate [Bishop and White, 1976; Trahar, 1981; Warren, 1985]. Factors that influence the amount of water to overflow include:

(i) bubble size [Cliff et al., 1978]
(ii) gas rate [Engelbrecht and Woodburn, 1975]
(iii) froth depth [Engelbrecht and Woodburn, 1975]
(iv) frother type [Subrahmanyam and Forssberg, 1988; Ekmekçiet al., 2003]

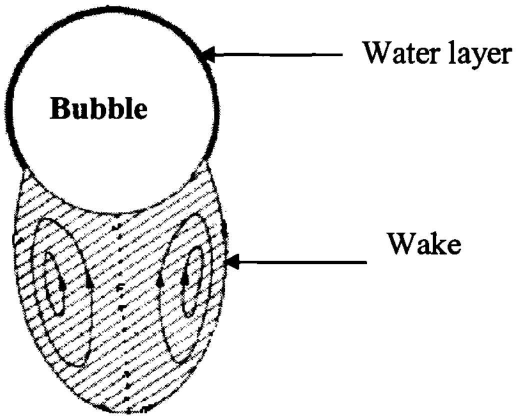

FIGURE 1.2: *Schematic of bubble carrying water [Smith and Warren, 1989 (Reprinted from Frothing in flotation 1, Laskowski J.S., Entrainment of particles into flotation froths, 1989 with permission from Gordon and Breach Science Publishers)]*

1.2 FROTHERS

Frothers are chemical reagents employed in flotation to aid the formation of fine bubbles and a stable froth. They have a heteropolar structure that causes them to adsorb at an air-water interface (i.e., bubble surface). This in turn stabilizes a water film on the bubble surface, which helps retard coalescence (the coming together of two or more bubbles to form one big bubble). Different frother types have been found to influence the amount of water and gangue entering the froth zone [Subrahmanyam and Forssberg, 1988], but there is no systematic quantification of the effect of frother type.

There are three main frother types used commercially in the mineral industry:

(i) Alcohols e.g. Methyl isobutyl carbinol (MIBC)
(ii) Polyglycols e.g. Dowfroth 250
(iii) Alkoxy-substituted paraffins e.g. 1.1.3 Tri-ethoxybutane (TEB).

The criterion for selecting frothers has been changing over the years. In the past, the focus was based mainly on cost, availability and environmental friendliness. Even though these factors are still important others related to performance, like fineness of bubble size dispersion and quality of froth produced are increasingly considered. To select frothers for industrial applications empirical tests involving laboratory batch flotation tests are normally conducted. There is not yet an accepted method for characterizing frothers for use in flotation. A number of characterizing techniques in the literature refer only to froth properties [Bikerman, 1938; Sun, 1952; McLaughlin et al., 1993; Iglesias et al., 1990]. More recently Laskowski and co-workers [Sweet et al., 1997; Cho and Laskowski, 2002; Laskowski, 2003; Laskowski et al., 2003] have combined bubble size reduction and froth properties to characterize frothers. What continues to be lacking is a full understanding of the mechanism(s) by which frothers prevent coalescence, and building from this, how to achieve the desired frother function.

1.3 HYPOTHESIS AND ORGANIZATION OF THESIS

1.3.1 Hypothesis and objectives

Frothers produce fine bubbles to enhance flotation rate and promote froth stability. These same bubbles that transport mineral particles also carry water. The recovery of water governs the recovery of gangue particles by entrainment, which is detrimental to the concentrate grade. Understanding water recovery in determining metallurgical (grade and recovery) performance is, therefore, second only to understanding particle recovery. It is hypothesized that the water carried by bubbles depends on frother type. This suggests a method to characterize frothers based on the water carrying capacity of the bubbles they help produce.

The objective of this work is to devise a way to measure bubble water carrying rate and relate to frother chemistry independent of other factors that influence the water carrying rate, notably bubble size, gas rate and froth height.

1.3.2 Organization of thesis

Chapter 1 gives the general overview of flotation and frothers and introduces the hypothesis and objectives of this Masters work. The literature review is divided in two parts; Chapter 2 is a review of frother chemistry, water recovery and gas dispersion parameters and Chapter 3 reviews frother characterization techniques. A description of the bubble column, calibration procedures and measurement techniques are outlined in Chapter 4. Frother characterization by water carrying rate with gas holdup and bubble surface area flux as independent variables is given is Chapter 5 and Chapter 6, respectively. Discussion, bringing the diverse points together, constitutes Chapter 7; and lastly, conclusions and recommendations for future work are included Chapter 8.

CHAPTER TWO

LITERATURE REVIEW

The importance of bubble size in controlling flotation efficiency has long been recognized and summarized in various reviews [Ahmed and Jameson, 1985; Dobby and Finch, 1986; Yoon and Luttrell, 1986; Fuerstanau, 1999]. A key factor controlling bubble size is the presence of frother (Harris, 1976). Frothers function by retarding coalescence. Coalescence determines the final size of bubbles and occurs virtually coincident with bubble production [Espinosa-Gomez et al., 1987; Hofmeier et al., 1995; Comely et al., 2002].

2.1 FROTHERS

Frothers belong to a group of chemicals known as surfactants or surface-active reagents. Frother molecules comprise two groups, one polar the other non-polar. The non-polar group is a hydrocarbon chain that can either be straight, branched or cyclic. The polar group could be a hydroxyl (OH), carbonyl (-C=O-), ester (-COOR-), carboxyl (-COOH), amine ($-NH_2$), nitrile (-CN), phosphate ($=PO_4$), or sulphate ($=SO_4$) [Booth and Freyberger, 1953; Wrobel, 1953, Laskowski, 1998]. The heteropolar structure causes frothers to preferentially adsorb at an air-water interface. At the moment of bubble generation, frother molecules adsorb on the bubble surface with the hydrocarbon chain on the airside and the polar group on the waterside where it hydrogen bonds with water molecules. This orientation is depicted in Figure 2.1 for MIBC (methyl isobutyl carbinol).

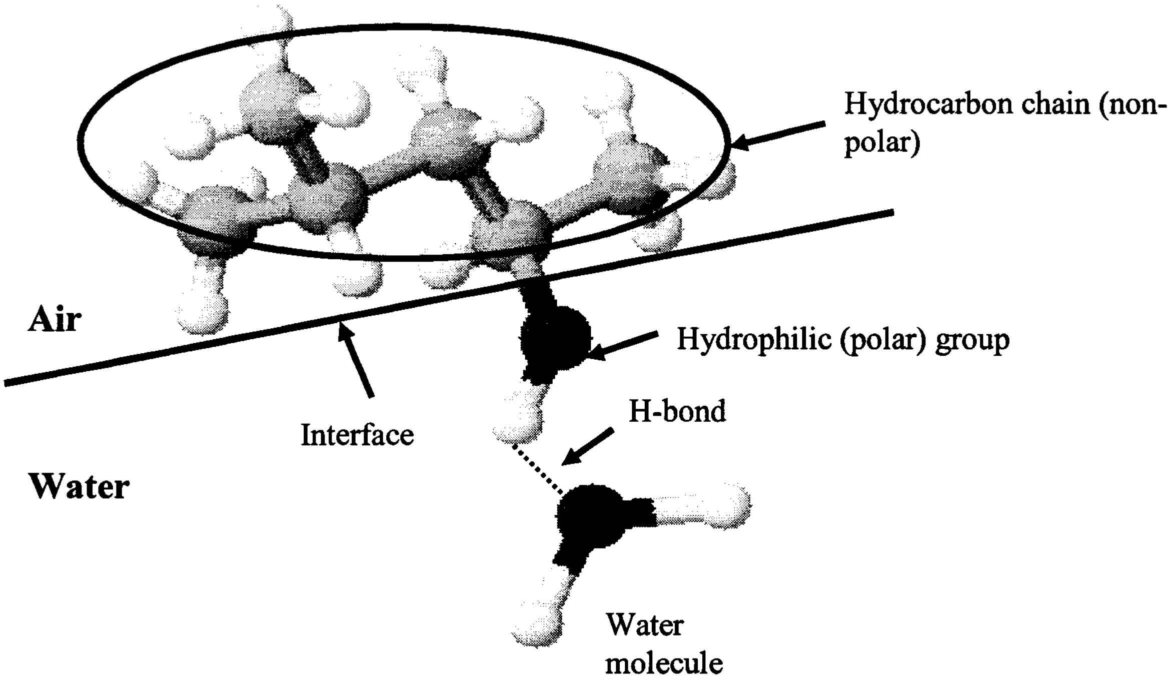

FIGURE 2.1: *Typical structure and orientation of frother molecule (MIBC in this case) at the air-water interface (i.e., bubble surface) (drawn using ACDlabs© software).*

One manifestation of adsorption is the lowering of surface tension with an increase in bulk concentration. The change in surface tension is related to the adsorption density as defined by the Gibbs equation [Wrobel, 1953, Booth and Freyberger, 1953, Sutherland and Wark, 1955]:

$$\Gamma = -\frac{C}{RT} * \frac{d\sigma}{dC} \tag{2.1}$$

where Γ = excess concentration of molecules adsorbed at the interface (adsorption density).

C = bulk concentration of solute molecules

σ = surface tension

R = gas constant

T = absolute temperature

The slope dσ/dC defines the surface activity of a surfactant. According to Traube's rule the activity increases threefold with each CH_2 group added to the hydrocarbon chain [Booth and Freyberger, 1962].

In addition to lowering surface tension, frothers also prevent coalescence, another surface related property. There are several mechanisms proposed. One mechanism is that the hydrogen bonding with water molecules forms a stabilized water film around the bubble (Figure 2.2). The water film is divided into two parts [Rödel, 1981]:

(i) an ordered boundary layer or capillary film which is tightly bound to the bubble and is immobile, and

(ii) a free flowing film, which is loosely bound.

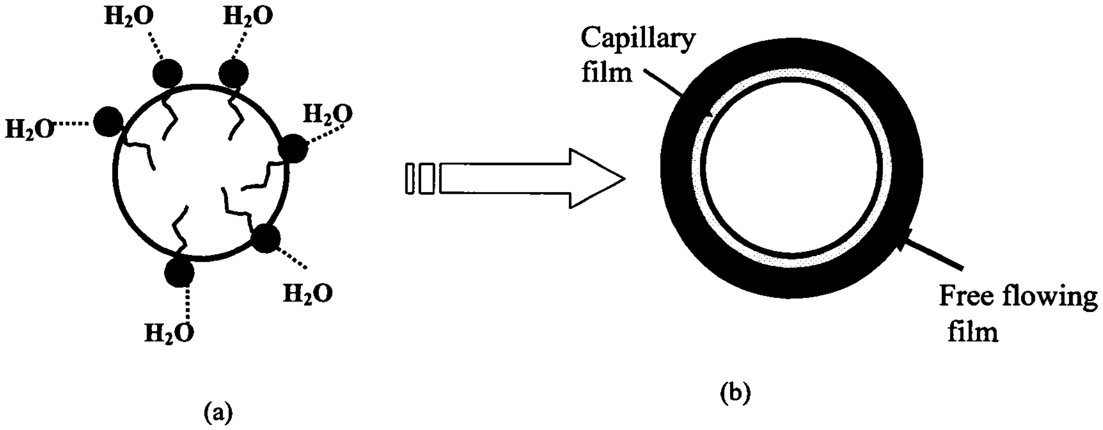

FIGURE 2.2: *(a) Frother molecules adsorb on bubble surface and hydrogen bond with water molecules resulting in (b) a water film around the bubble.*

The capillary film in particular resists drainage and thus retards coalescence. The mechanism is akin to considering the bubbles (surface) as hydrophilic [Finch et al., 2003] and, analogous to hydrophilic (surface) particles in water, they tend to repel and remain dispersed [Hunter, 1987; Ducker et al., 1992]. That is, frothers make bubbles behave like stabilized particle dispersions.

A second mechanism relates to surface tension driven phenomena. Upon drainage of the intervening water layer, prompted for example by bubble collision, a drag on the bubble surface is induced causing the surface to flow with the water. This causes a local decrease in frother concentration, i.e., a local increase in surface tension. Thus a surface tension gradient is produced which opposes the motion of the surface (Gibbs elasticity effect). The surface tension gradient can then induce a flow in the adjacent water layer in the direction of increasing surface tension reversing the outflow of water (Marangoni effect). Together these two effects oppose film drainage and retard coalescence [Harris, 1982].

The same forces that prevent coalescence and preserve fine bubbles also promote formation of a stable froth. The stability of the froth is dependent on the surface elasticity and the surface viscosity of the adjoining water layer. The adsorbed frother controls the visco-elastic properties of the water layer and hence influences the drainage rate and stability of foams.

2.1.1 Practical aspects of frothers

Apart from these anti-coalescence attributes, to be of commercial interest frothers must also:

a) produce a froth that is able to transport particles to the launder but must subsequently break readily to permit further processing
b) create a froth that allows further separation of valuable minerals from gangue through drainage of water
c) be relatively cheap, abundant and environmentally safe
d) not ionize and should have a low sensitivity to pH changes to avoid complications of interacting with the collector
e) readily disperse in aqueous medium (but not necessarily be readily soluble)
f) not have collecting properties.

2.1.2 Frother chemistry and frother classification

There are three main groups of frothers that are widely employed in the mineral industry: alcohol, alkoxy substituted alcohol and polyglycol types. Table 1:1 summarizes some properties of various frothers.

(a) Alcohols

There are 3 subgroups in the alcohol group, linear aliphatic, cyclic and aromatic. Linear aliphatic alcohols include both linear and branched forms that have a carbon chain length (C) of 5 to 8 atoms (if C<5 frother related properties are too weak; if C>8 the molecule is difficult to dissolve/disperse). The functional group of the alcohols is the single hydroxyl group. The general characteristics of linear aliphatic alcohols compared to the other frother types include [Riggs, 1986; Klimpel and Hansen, 1988, Crozier and Klimpel, 1989]:

(i) fast kinetics i.e., rapid recovery of particles
(ii) brittle froth
(iii) low water retention resulting in more selectivity
(iv) limited water solubility (0.3-0.9%) [Riggs, 1986]
(v) relatively shallow froth depths.

Cyclic and aromatic alcohols are much less soluble in water (0.2-0.5%) than linear alcohols and are less sensitive to pH. Cyclic alcohols are chosen over linear alcohols when a more elastic and persistent froth is desired.

(b) Alkoxy-type frothers

1,1,3-Triethoxybutane (TEB) is the common frother in this group, developed and widely used in South Africa [Klimpel and Hansen, 1988, Crozier and Klimpel, 1989]. It is a refinement of the alcohol group and overall has similar characteristics.

(c) Polyglycol type frothers

This type of frother divides into two groups: polyglycol ethers and polyglycols. General characteristics of polyglycol ethers include [Riggs, 1986]:

(i) Total water solubility resulting in low dosages being utilized.
(ii) Good froth depth
(iii) Relatively stable froth compared to alcohols at a fixed dosage.
(iv) High water retention
(v) Persistent froth
(vi) Low sensitivity to pH changes.

Polyglycols perform much like the polyglycol ethers but more intensely. The disadvantage of polyglycols is the high water retention, which could make them less selective than polyglycol ethers. However this character of polyglycols could be advantageous when recovering coarse particles [Riggs, 1986; Klimpel and Hansen, 1988].

Another parameter that is used to classify frothers is the hydrophile-lipophile balance (HLB number). The HLB number is a ratio of the hydrophilic to hydrophobic (lipophilic) parts of a frother. It determines whether the hydrophilic group will interact with water molecules. The solubility of frother is thus related to the HLB; frothers with a high HLB are more hydrophilic and therefore more soluble in water.

TABLE 2:1: *Classification of frothers. R_1 and R_2 = H or C_nH_{2n+1}, [Crozier, 1992; Rao, 2004]*

	Sub groups	Typical Example	Mol wt g/mol	Solub. g/l	Density g/ml
Alcohols R-OH	Aliphatic	MIBC 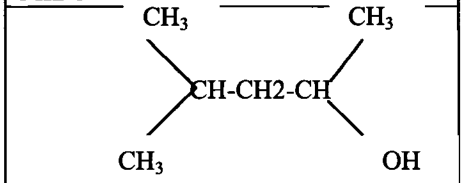	102	17	0.808
		2-Ethyl Hexanol/ Heptanol 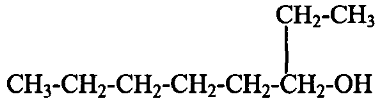 $CH_3\text{-}CH_2\text{-}CH_2\text{-}CH_2\text{-}CH_2\text{-}\overset{CH_2\text{-}CH_3}{\overset{\mid}{C}}H_2\text{-}OH$	116	1.8	0.822
	Cyclic	a-Terpineol 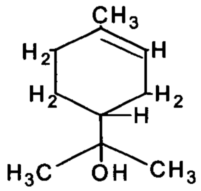	154	2.5	0.9336
	Aromatic	o-Cresol 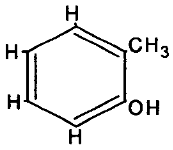 2,3-Xylenol 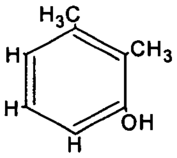		1.7	1.01-1.04
Alkoxy paraffins		1,1,3 Triethoxybutane 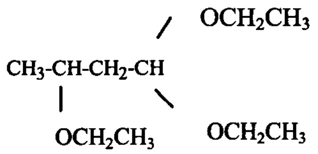 $CH_3\text{-}\underset{\substack{\mid\\OCH_2CH_3}}{CH}\text{-}CH_2\text{-}\overset{/\ OCH_2CH_3}{\underset{\backslash\ OCH_2CH_3}{CH}}$	190	~8	
Polyglycol-type		Dow froth 250 $CH_3(PO)_4OH$	250	Total	0.98
R-$(O\text{-}R_2)_n$-OH		Dowfroth 1012 $CH_3(PO)_{6..3}OH$	400	Total	0.988

2.3 WATER TRANSPORT

The amount of water reporting to the concentrate controls gangue recovery [Jowett, 1966; Bishop and White, 1976; Trahar and Warren, 1976, Lynch et al., 1981, Warren, 1985; Neethling and Cilliers, 2002]. Two general mechanisms have been advanced to explain the presence of free gangue particles in the concentrate [Smith and Warren, 1989]:

(i) transport in the inter-bubble water (entrainment)
(ii) recovery via aggregates attached to air bubbles (entrapment).

Research has shown that entrainment is the major mechanism [Engelbrecht and Woodburn, 1975; Trahar, 1981;Warren, 1985; Smith and Warren, 1989; George et al., 2004]. There are two mechanisms that are frequently invoked to explain the transport of water into the froth:

(i) Water is carried upward in the water film surrounding the bubble (Figure 2.3) [Gaudin, 1957]
(ii) Water is transported in the wake of the ascending air bubble [Yianatos et al., 1986b; George et al., 2004]

Smith and Warren (1989) object to these mechanisms, basing their argument on three facts:

(i) The formation of a bubble wake occurs over a limited range of hydrodynamic conditions and it is impossible to imagine such conditions existing at the base of every froth column.
(ii) Inside the froth, the existence of a wake is doubtful due to the close packing of bubbles.
(iii) The actual thickness of the boundary film as a bubble crosses the interface is not known.

They proposed a mechanism where water is mechanically pushed into the froth by ascending swarms of bubbles (Figure 2.4).

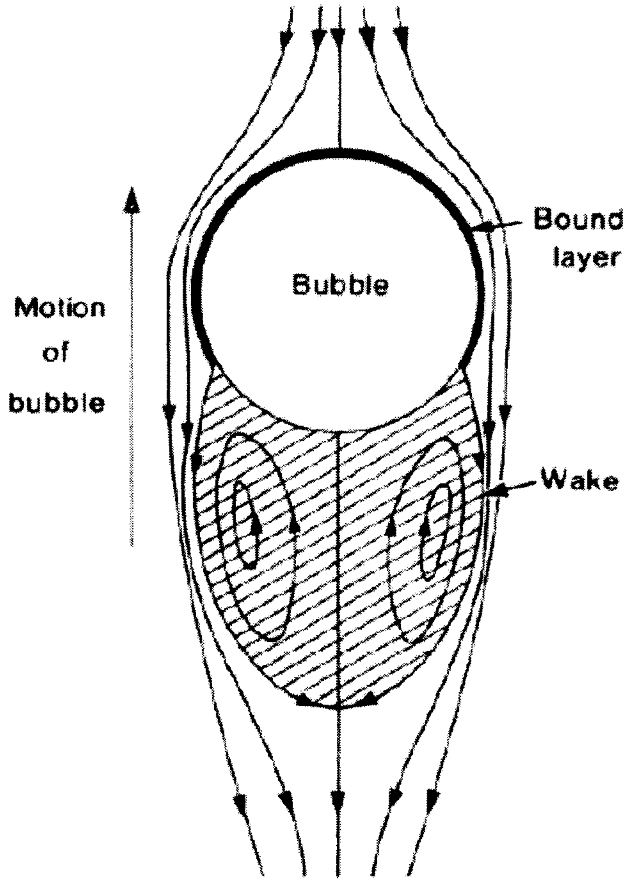

FIGURE 2.3: *Ascending bubble with bound water layer and an attached wake [Smith and Warren, 1989 (Reprinted from Frothing in flotation 1, Laskowski J.S., Entrainment of particles into flotation froths, 1989 with permission from Gordon and Breach Science Publishers)]*

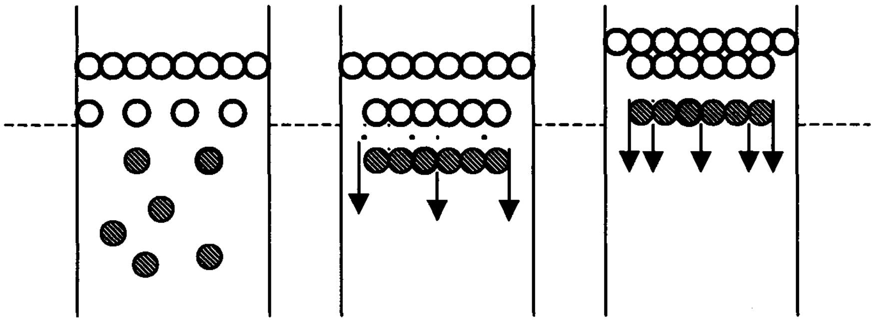

FIGURE 2.4: *Water mechanically pushed into the froth by successive layers of ascending bubbles [Smith and Warren, 1989]*

One way to estimate the rate of water carried into the froth (C_{wf}) is to assume it is a function of rate of bubble surface passing through the cell multiplied by an equivalent water boundary layer thickness (δ),

$$C_{wf} = n*S*\delta \tag{2.2}$$

where n is the number of bubbles per unit time (($=\frac{Q_g}{V_b}$), Q_g being the volumetric flowrate of air (e.g., m^3/s) and V_b the volume of a single bubble ($=\frac{\pi d_b^3}{6}$)), and S is the surface area per bubble (πd_b^2). Equation 2.2 simplifies to (assuming spherical bubbles):

$$C_{wf} = \frac{6Q_g * \delta}{d_b} \tag{2.3}$$

Dividing equation 2.3 by the cross sectional area of the flotation cell (A, m^2) gives

$$J_{wf} = 6\frac{J_g}{d_b} * \delta \tag{2.4}$$

$$J_{wf} = S_b * \delta \tag{2.5}$$

where J_g is the superficial gas velocity (Q_g/A) and S_b is the bubble surface area flux. Xu et al., (1991) showed that the volume of water transported to the froth did vary with S_b but did not include δ. Bascur and Herbst (1982) used Levich's (1962) boundary layer thickness correlations to estimate δ, namely:

$$\delta = \left(\frac{\nu * \left(\frac{d_b}{2} \right)}{U_{sb}} \right)^{\frac{1}{2}} \tag{2.6}$$

where ν is the kinematic viscosity and U_{sb} is the bubble rise velocity. For Re >> 1 (Reynolds number), the thickness of the boundary layer is small compared to the bubble radius [Levich, 1962]. Hydration effects at the bubble-water interface and agitation conditions in the slurry were considered to control the magnitude of the boundary layer [Bascur and Herbst, 1982]. No factor relating to frother type was included.

A possible alternative estimation route for C_{wf} is based on the wake volume. From numerical analysis, George et al. (2004) correlated the wake volume (Vol_w) with the bubble volume (V_b) and the Reynolds number (Re)

$$Vol_w = V_b\left[0.045\,\mathrm{Re}^{0.649} - 0.314\right] \tag{2.7}$$

for $20 \le \mathrm{Re} \le 400$.

In the absence of a froth layer C_{wf} is equal to water overflow rate (Q_{wo}). In the presence of froth, drainage effects have to be considered. Cilliers and coworkers [Neethling et al., 2000; Neethling and Cilliers, 2002; Neethling et al., 2003] are developing fundamental models to predict water overflow from flowing foam (2-phase froth). Their analysis takes into account foam drainage and the number of unburst bubbles that overflow (α). They found that if:

$$\alpha < \tfrac{1}{2}: \; J_{wo} = \frac{Q_{wo}}{A} = \frac{J_g^2 \lambda}{k_1}(1-\alpha)\alpha \tag{2.8}$$

$$\alpha \ge \tfrac{1}{2}: \; J_{wo} = \frac{J_g^2 \lambda}{4k_1} \tag{2.9}$$

where k_1 is a constant, a balance of gravity and viscous forces, and λ is the length of Plateau borders per volume of foam, A is the column cross sectional area and J_g is the superficial gas rate. Again, no effect of frother type is included. There is, presumably, a relationship between J_{wf} and J_{wo}

2.3.1 Effect of frothers on bubble size and boundary layer thickness

Frother type and concentration affects bubble size (d_b) and probably boundary layer thickness (δ). Over a certain range an increase in frother concentration decreases bubble size and therefore increases the overall bubble surface area rate and hence volume of water carried into the froth [Asplin et al., 1998]. Gelinas et al. (2005) measured the boundary layer thickness (δ) of two industrial frothers, MIBC and Dowfroth 250, using interferometry. They found that Dowfroth 250 gave a thicker water film than MIBC. These micro-scale measurements confirm the macroscopic observation that Dowfroth 250 has higher water retention than MIBC [Riggs, 1986; Klimpel and Hansen, 1988]. The difference was attributed to the molecular structure of the two frothers, which influence the way they hydrogen bond with and order (stabilize) water molecules. Using infrared analysis of bubble films, Gelinas et al. (2005) distinguished the bound and free water layers.

2.3.2 Effect of gas rate on water overflow

An increase in gas rate increases the number of bubbles crossing the collection-froth zone interface thus pulling more water and gangue particles into the froth [Lynch et al., 1981; Kaya and Laplante, 1986]. Engelbrecht and Woodburn (1975) observed a linear relationship between water recovery and gas rate. A linear relationship is expected if the increase in gas rate has little effect on bubble size distribution or the effective boundary layer thickness. Neethling et al., (2003) found that for a constant bubble size the water overflow rate is proportional to gas rate squared (equation 2.8 and 2.9). Some authors [Moys, 1978; Cutting and Devenish, 1982] found that an increase in gas rate while increasing water recovery also increased concentrate grade. High gas rates are associated with more mixing and higher water content in the froth, which enable particles (especially coarse ones) to drain more freely. Generally, however, the overall net water recovery and particle entrainment increase with gas rate and decrease concentrate grade [Ross, 2001; Cooper et al., 2004].

2.3.3 Effect of froth height

Varying froth height has been used as one means of controlling entrainment and hence concentrate grade. An increase in froth height increases the residence time of bubbles in the froth resulting in increased particle drainage. Engelbrecht and Woodburn (1975) reported a decrease in water recovery with increasing froth height and a concomitant decrease in fine silica recovery.

2.4 GAS DISPERSION PARAMETERS

In flotation the hydrodynamic variables that characterize gas dispersion in the pulp and correlate to metallurgical performance are superficial gas velocity (J_g) bubble size distribution (d_b), gas holdup (ε_g) and bubble surface area flux (S_b). In mechanical cells the power number and airflow number should also be included [Harris, 1976].

2.4.1 Superficial Gas Velocity

Superficial gas velocity, or simply gas rate (J_g, cm/s) is defined as the volumetric flowrate (Q_g, cm^3/s) of air per cross sectional area (A, cm^2) of flotation machine ($J_g = Q_g/A$). Typical ranges in flotation systems are 0.5-2.5cm/s depending on factors such as bubble size and slurry rheology.

2.4.2 Bubble Size

The rate of tranport of solid particles and water depend on size, velocity of rise and interaction of individual bubbles with each other and with particles. Bubble size distribution is an important factor determining how well air is dispersed in a liquid (slurry) phase. Coalescence is one mechanism that reduces the dispersion efficiency of a flotation system [Cho and Laskowski, 2002]. The Sauter mean diameter (d_{32}) is commonly used to quote bubble size. The typical bubble size in flotation is 0.5-2.5mm [Gorain et al., 1995].

2.4.2.1 Effect of frothers on bubble size

Frothers have a pronounced impact on reducing bubble size up to a certain concentration above which further addition of frother appears to have no effect [Finch and Dobby, 1990]. Figure 2.5 illustrates the effect of frother concentration on bubble size. A decrease in coalescence is the accepted explanation of the decrease in bubble size with increasing frother concentration. After a certain concentration, recently tagged the critical coalescence concentration (CCC), a constant bubble size is obtained implying that coalescence is now minimal. Different frothers reach CCC at different concentration [Sweet et al., 1997; Laskowski et al., 1998]. A number of investigators have tried to link the ability to reduce bubble size to surface tension. Lower surface tension values are usually associated with higher frother concentration that result in smaller bubbles. Aldrich and Feng (2000) found that MIBC solutions with higher surface tension values than Dowfroth 200 nevertheless produced smaller bubbles. Over the concentration ranges used in flotation surface tension hardly changes even though bubble size reduction is taking place. In the case of salts, above a certain concentration, coalescence is also retarded [Klassen and Mokrousov, 1963] but here solution surface tension increases. Prevention of coalescence is not related simply to surface tension.

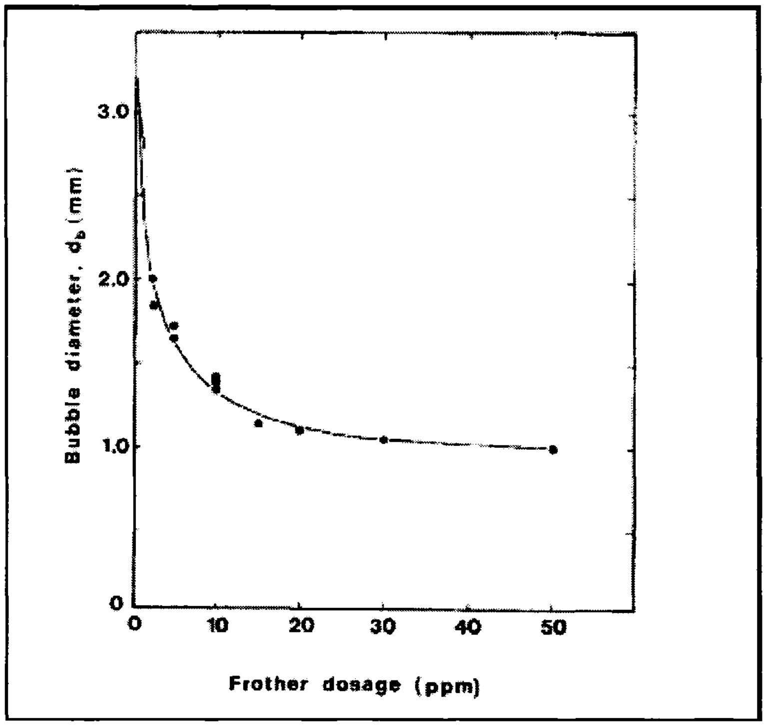

FIGURE 2.5: *Bubble size versus frother concentration (Dowfroth 250C) [Finch and Dobby, 1990 (Reprinted from Column flotation, Finch J.A. and Dobby, G.S., Gas holdup and bubbly flow p15-21, Pergamon Press, New York, 1990 with permission from Elsevier)]*

2.4.3 Gas holdup

Gas holdup is the volume fraction occupied by gas at any point in a flotation cell (in this case). It is a function of a number of interactive variables involving chemical (e.g., frother type and concentration), operational (gas rate) and machine (bubble generation system) factors. It is the simplest gas dispersion parameter to measure that combines the influences of bubble size and gas rate.

At constant gas rate smaller bubbles ($\leq$ 2mm) rise more slowly resulting in higher gas holdup. Figure 2.6 illustrates the effect of both frother concentration (to reduce bubble size) and gas rate on gas holdup. Zhou et al. (1993) found that for different frother systems, a higher gas holdup did not necessarily imply that a smaller bubble size was produced; that is, there appeared to be an effect of frother type. Sam et al. (1996) measured the terminal velocity of a single bubble in different frother systems and found that the terminal velocity was dependent on frother type.

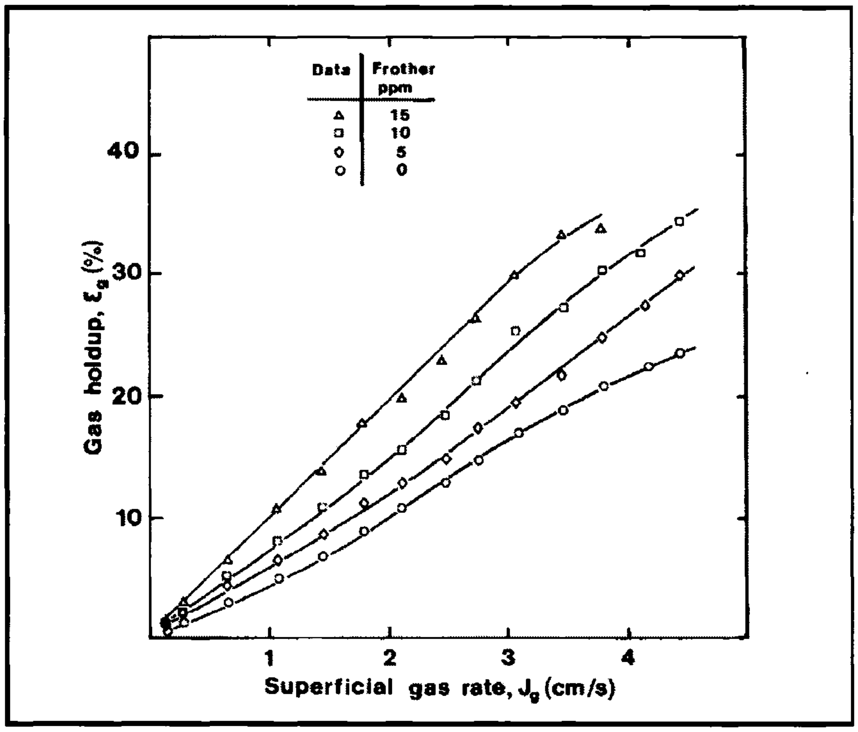

FIGURE 2.6: *Effect of frother concentration (Dowfroth 250C) and gas rate on gas holdup [Finch and Dobby, 1990 (Reprinted from Column flotation, Finch J.A. and Dobby, G.S., Gas holdup and bubbly flow p15-21, Pergamon Press, New York, 1990 with permission from Elsevier)]*

2.4.4 Bubble surface area flux

Bubble surface area flux (S_b) is emerging as one of the most useful variables to quantify gas dispersion [Gomez and Finch, 2002]. It is defined as the amount of bubble surface area delivered per unit time and cell cross-sectional area, and is given by

$$S_b = \frac{6J_g}{d_b} \tag{2.8}$$

where J_g is the superficial gas velocity and d_b is the Sauter mean bubble diameter of the distribution. Gorain et al. (1997) and Hernandez et al. (2003) found that the flotation rate constant was directly proportional to S_b. Increasing J_g, and/or decreasing d_b can increase S_b. In practice, an increase in J_g increases bubble size giving a trade-off, this being one reason why there is an optimum J_g in flotation [Finch and Dobby, 1991].

CHAPTER 3

FROTHER CHARACTERIZATION TECHNIQUES

Frothers differ in their influence on flotation according to their chemistry [Malysa et al., 1987] hence the desire to characterize especially using properties that relate to flotation. Frother characterization techniques exploit some of the essential tasks of frothers, for example formation of a stable foam[1] and extent of bubble size reduction. A number of methods over the years have been developed to assess foam formation [Bikerman, 1938; Sun, 1952; Malysa et al., 1976; Barbian 2003; Barbian et al., 2003]. In general, two types of tests are used, dynamic tests and static tests. In a dynamic test, air is supplied continuously and foam is allowed to grow until steady state is reached where the rate of formation is in equilibrium with rate of decay (bubble bursting). In static tests the rate of foam formation is zero: once the foam is formed, it is allowed to collapse without further gas input or agitation.

3.1 REVIEW

3.1.1 Dynamic tests

Probably the most widely known foam test is that of Bikerman (1938). He defined a unit of foaminess Σ, as the average lifetime of a bubble in foam. The idea was to utilize Σ as a definite physical property of a frother solution just like its density and viscosity. In the test, air is dispersed through a sparger in a cylinder containing solution and the foam is allowed to grow until equilibrium is reached. Foam height or volume is then measured. The unit of foaminess (Σ) or foam stability factor (as now normally referred to) is given by

---

[1] Foam and froth are normally used interchangeably, however foam will be used here to refer to a two-phase (no solids) froth.

$$\Sigma = \frac{V_f t}{V_g} \Longrightarrow \Sigma = \frac{V_f}{Q_g} \tag{3.1}$$

where V_f is the volume of foam and V_g is the volume of gas passed through the column in time t, i.e., Q_g is the gas volumetric flowrate ($Q_g = V_g/t$). Σ was found to be independent of the gas flowrate (if the gas rate was neither too low nor too high), the shape of the container and the average pore size of sparger. Bikerman made two assumptions:

(a) the volume of the liquid in the foam is negligible

(b) bubble coalescence in foam is negligible.

The first assumption does not always hold, particularly as some foams are notably 'wet'and the second is reasonable for foam layers just above the foam-liquid interface but does not hold for the top layers.

Barbian et al. (2003) developed a technique that tries to relate the unit of foaminess to flotation performance. They monitored froth growth with time and found the relationship

$$H_f = H_{\max}(1 - e^{t/\tau}) \tag{3.2}$$

where H_{max} is the total foam height, H_f is the froth height at time t and τ is the characteristic average bubble lifetime (i.e., Σ). They postulated that the froth rise velocity is related to the fraction of air overflowing as unburst bubbles. Since a fraction of bubbles burst in the froth column, the rising velocity at each height decreases by a factor of β (H) that represents the fraction of air remaining in the froth at a given height H (t). Equation 3.3 shows how β can be determined as a function of froth height,

$$\beta = 1 - \frac{H(t)}{H_{\max}} \tag{3.3}$$

The value of β was used to quantify the effect of operational variables on froth stability since the relationship between H (t) and H_{max} will be influenced by factors such as frother type and concentration, airflow rate and solids loading.

Watkins (1973) suggested using a conical vessel instead of a cylinder and proved it gave better reproducibility. Ross and Suzin (1985) further developed Watkins' idea but went on to observe that a test should produce foam and measure stability under conditions similar to those of its ultimate application.

Sun (1952) designed a frother-meter capable of measuring the foaming characteristics of pine oils and other frothing reagents. He defined a foamability index (FI) as the ratio of foam volume produced from a solution of the frother tested to the volume of foam produced from a chosen standard solution of n-hexyl-alcohol. He also defined a stability index (SI) as the ratio of the persistence (time for foam to collapse) of the frother under test to the standard frother.

Malysa et al. (1978) defined retention time (rt) as a measure of the bubble lifetime in the whole system (solution + foam). Physically, rt was defined as the average time necessary for unit gas volume to pass from the bottom of the column where bubbles are produced to the highest foam layer where bubbles rupture. Graphically rt is the slope of the linear section of the dependence of the total gas volume contained in the system, V_g, on the gas flow rate, Q_g [Malysa et al., 1981],

$$\mathrm{rt} = \frac{\Delta V_g}{\Delta Q_g} \tag{3.4}$$

Like the Bikerman unit of foaminess, rt is independent of the gas flow rate and the dimension of the measuring equipment. It is linked to Σ by equation 3.5:

$$\mathrm{rt} = \Sigma + \frac{\Delta V_l}{\Delta Q_g} \tag{3.5}$$

where ΔV_l is the variation in volume of the liquid phase (solution + bubbles) with a change in gas flow rate ΔQ_g. The rt value includes the unit of foaminess Σ and the change in volume of liquid which eliminates Bikerman's assumption that the solution content in the foam is zero.

Malysa et al. (1985) defined a dynamic foamability index (DFI) as the limiting slope of the rt dependence on concentration (c) for $c \to 0$.

$$\mathrm{DFI} = \left(\frac{\partial rt}{\partial c}\right)_{c=0} \tag{3.6}$$

DFI enables a comparison of frothers and their action to be made under conditions of identical foamability. Equation 3.7 can be fitted to rt vs concentration (c) in order to estimate the initial slope (i.e., when c =0)

$$rt - 2.4 = (rt_\infty)^n \left[1 - e^{-k_n c}\right] \tag{3.7}$$

where n is the number of carbon atoms in the molecule homologue, k_n and rt^n_∞ are constants dependent on surfactant properties, for example frother type and surface activity. The $(rt_\infty)^n$ is the value of rt for $c \to \infty$ and 2.4 is the value of rt for distilled water [Wantke et al.,1994]. After expansion into a power series for $c \to 0$, equation 3.7 becomes [Laskowski, 1998]

$$rt - 2.4 = rt_\infty \cdot k \cdot c$$

$$DFI = rt_\infty \cdot k \tag{3.8}$$

Malysa et al. (1985) related foamability (rt) to surface elasticity of a bubble film. The effective surface elasticity was measured using the oscillating bubble motion method i.e., the bubble was made to oscillate with known amplitude and frequency immediately after formation. They found that the effective surface elasticity (E_{eff}) and rt varied in a similar way with the chain length in n-alcohol molecules. Both E_{eff} and rt showed dependences on carbon chain length with the maximum observed for C_6-C_8.

Comely et al. (2002) characterized frothers using dynamic surface tension measurements using a modified bubble pressure technique. The results revealed a trend in the adsorption density of frothers of the same family, which they used to interpret the behaviour of surfactants in flotation.

Sweet et al. (1997) characterized different frothers using the DFI and $C_{0.6}$, the concentration at which the Sauter mean diameter is reduced to 0.6 times that in water. They found that normal alcohols behaved differently from branched chain alcohols. For n-alcohols the correlation is given by:

$$\frac{C_{0.6}}{0.059} = DFI^{a_1} \text{ , } a_1 = 0.64 \tag{3.9}$$

and for branched chain alcohols

$$\frac{C_{0.6}}{65.91} = DFI^{a_2} \text{, } a_2 = 1.16 \tag{3.10}$$

3.1.2 Static tests

Iglesias et al. (1995) modified Bikerman's method by switching off gas once the dynamic equilibrium height was reached. The decay of foam volume was measured with time t; a parameter $t_{1/2}$ was defined as the time for the foam to decay to half the original height, H_o (for constant cross sectional area). This parameter was used to characterize the persistence of the foam produced from a solution of known concentration. The rate of height change is therefore given by

$$\frac{\partial H_f}{\partial t} = -\frac{\alpha}{t} \tag{3.11}$$

Integrating equation 3.11 gives a linear relationship

$$H_f = -\alpha \log(t) + C \tag{3.12}$$

where α is the slope and C is the intercept. Taking $t_{1/2}$ as the reference time and foam height $H_{\frac{1}{2}} = {}^{H_f}\!/_{H_o}$, equation 3.12 can be written as:

$$\frac{H_f}{H_o} = -\alpha \log\left(\frac{t}{t_{1/2}}\right) + C \qquad (3.13)$$

where α is the decay constant. Plotting the dimensionless height against $\log\left(\frac{t}{t_{1/2}}\right)$ produces a straight line which passes through H_f/H_o = ½ and $\log\left(\frac{t}{t_{1/2}}\right)$ = 0. The value of α is constant for a given type of surfactant and concentration. McLaughlin et al. (1993) used almost the same method as Iglesias et al. (1990) but introduced an induction time (time elapsed between air termination and the start of froth collapse) and used α as the characterizing parameter instead. Their method was used on three phase froths.

Xu et al. (1990) proposed a new method of evaluating froth stability and foamability. Their argument is based on the fact that when frothers are compared at the same concentration they will produce different froth heights and hence different froth stabilities (different $t_{1/2}$). Foam heights were plotted against $t_{1/2}$ and a good linear correlation was obtained for different frothers. They found that alcohols (MIBC, n-heptanol, n-octanol and 2-octanol) had the same slope, which showed that they had almost the same foam stability. The position of a frother in the foam height-$t_{1/2}$ plot revealed the difference in foamabilities.

CHAPTER 4

EXPERIMENTAL

A bubble column was used to measure water carrying rate and relate to the gas dispersion parameters. The water carrying rate was quantified by measuring the water overflow rate per unit cross-sectional area (J_{wo}) at a given foam depth. The gas dispersion parameters measured were gas holdup, bubble size and gas rate. In this chapter a description of the column is given along with calibration procedures, measurements and characterization techniques

4.1 BUBBLE COLUMN

A specially designed column was constructed, 10cm internal diameter with eleven 2.5cm wide stainless steel ring electrodes flush mounted to the inner wall to make ten conductivity cells. The conductivity[1] cells were used to estimate gas holdup using Maxwell's model [Maxwell, 1892]. These signals were also used to control the solution-foam interface position (i.e., foam depth). The electrodes were separated by 7.5cm wide acrylic sections for the bottom part of the column (mainly below the foam, i.e., in the 'solution' zone) and 5cm wide acrylic sections for the upper part (foam zone). Figure 4.1 depicts the bubble column used. The column had the flexibility of changing the distance between each electrode by using different acrylic sections. The electrodes and acrylic sections were held together by three rods to make a column 105cm high. The electrodes were connected to a conductivity meter then to a data acquisition computer. The circuit board for the conductivity meter was purchased from Laval University.

The column was operated in continuous mode; the feed solution was introduced using a pump (Cole Palmer model 7520-25) and the liquid overflow recycled back to the feed

---

[1] See Appendix 1 for discussion of conductivity in this context.

solution tank. A calibrated mass flow meter was used to control the gas flow rate and a vertical porous sparger was used to generate air bubbles. A temperature sensor (Thermopar type K) was used to monitor temperature in the column in order to correct the conductivity values to the standard temperature of 25°C.

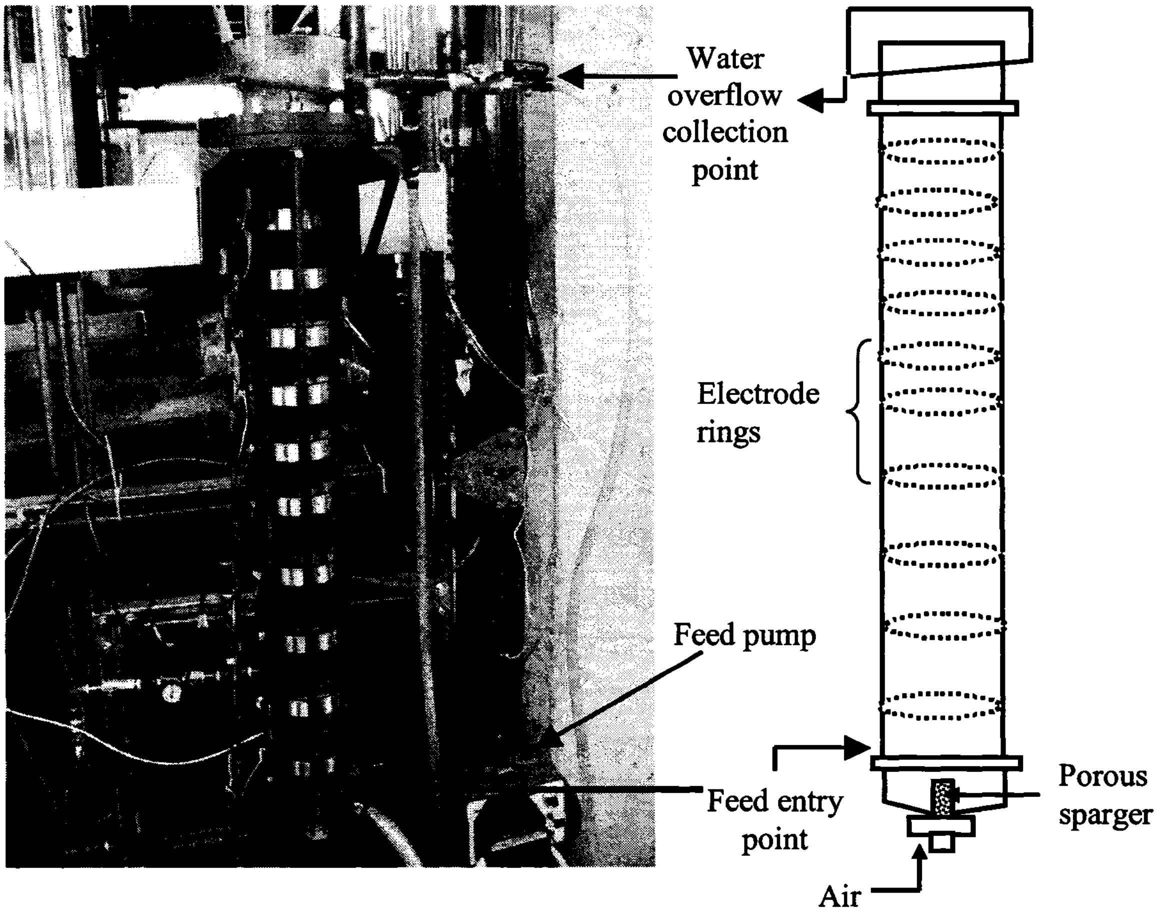

FIGURE 4.1: *The bubble column*

4.1.1 Calibrations

The conductivity cell constants were determined by comparing the conductivity values from the bubble column to a standard conductivity meter (Radiometer).

4.1.1.1 Radiometer calibration

Prior to using the Radiometer, the instrument was calibrated against 10 standard solutions (Fischer Scientific). Figure 4.2 shows the calibration curve obtained. A thermometer was used to check the solution temperature given by the built-in sensor of the Radiometer.

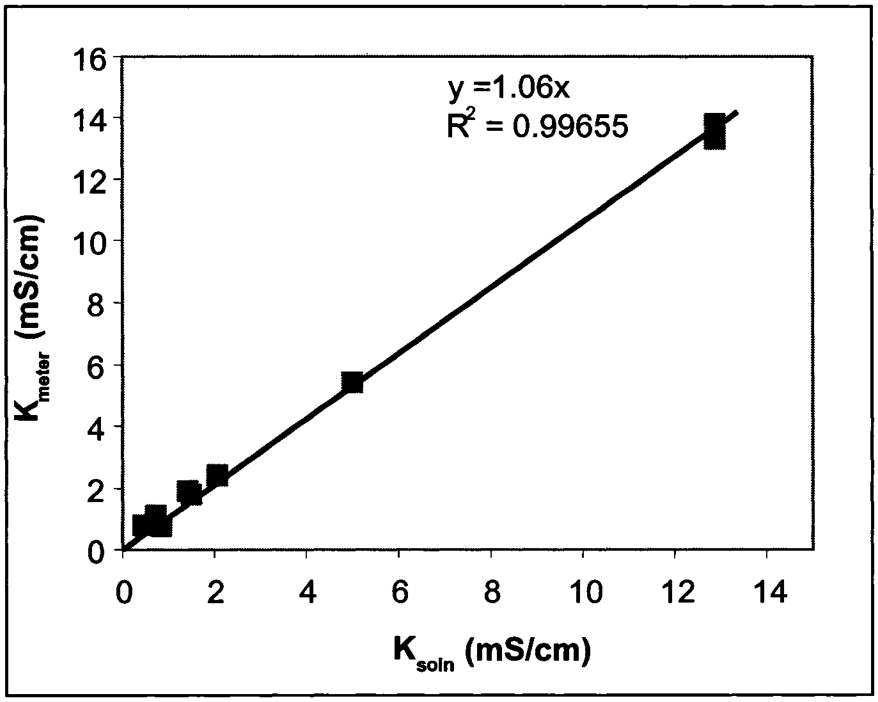

FIGURE 4.2: *Standard conductivity meter calibration (Radiometer). K_{meter} is the conductivity values from the Radiometer and K_{soln} are standard solutions*

4.1.1.2 Cell constant determination

Salt was added to cover a calibration range of 0.28mS/cm-0.70mS/cm. The salt solution was pumped into the column and the voltage output values obtained for each cell were plotted against the Radiometer conductivity values. The slope was then used to convert the voltage output to conductivity values. The cell constant determination data and the visual basic program used to calculate conductivity are given in Appendix 2.

4.2.2 Sparger selection

The sparger must meet the following criteria that were set:

(a) at least 7cm to35cm of foam must be produced with the weakest frother, n-pentanol.

(b) a clear solution-foam interface should be detected both visually and using a profile of conductivity values.

(c) the ratio $A_c/A_S \leq 1$ where A_c is column cross sectional area and A_s is the sparger surface area (to aid giving small bubbles [Xu et al., 1989; Finch and Dobby, 1990])

Three spargers with nominal porosity of 2µm, 5µm and 20µm were tested and for the 2µm porosity case three different lengths were used, giving A_c/A_S ratio of 1.04, 1.98 and 3.7, respectively. The 5µm sparger ($A_c/A_S = 1.98$) was chosen for most of the test work.

4.3 MEASUREMENTS

4.3.1 Gas holdup

In exploring factors that control water carrying rate, gas holdup, by reflecting both gas rate and bubble size was considered. Dispersion conductivity values (κ_d) compared to unaerated solution (κ_w) were used to calculate gas holdup using Maxwell's model for a non-conducting spherical dispersed phase (bubbles in this context) in a conducting continuous medium [Maxwell, 1892]

$$\varepsilon_g = \frac{1-\frac{\kappa_d}{\kappa_w}}{1+0.5\frac{\kappa_d}{\kappa_w}} \tag{4.1}$$

The gas holdup measurements from electrical conductivity were validated against an independent technique, based on differential pressure. Figure 4.3 shows the set up used.

The pressure method utilizes the difference in pressure (ΔP) between two tapping points separated by a distance L. Pressure transducers (Figure 4.3) or water manometers can be used to measure the pressure difference; in this case a differential pressure transducer was used. Point A was located about 10cm above the sparger and point B was at atmospheric pressure (P_{atm}). Gas holdup is then given by

$$\varepsilon_g = \frac{\Delta P(cmH_2O)}{\Delta L(cm)} \tag{4.2}$$

where ΔP is the pressure difference between point B (P_{atm}) and point A (P_A), and ΔL is the distance between tapping points. Figure 4.4 shows the correlation between gas holdup readings from pressure and conductivity. Conductivity values shown are the average from the 10 cells.

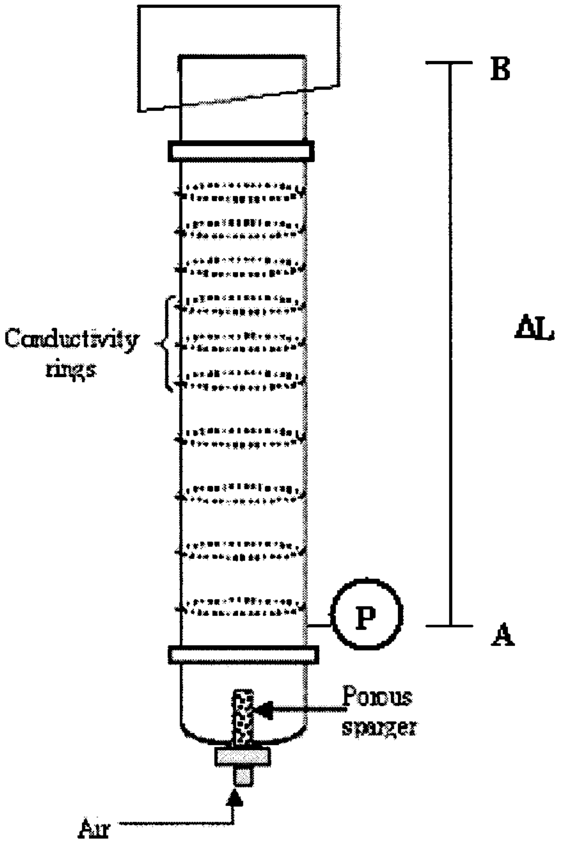

FIGURE 4.3: *Experimental set-up for gas holdup validation*

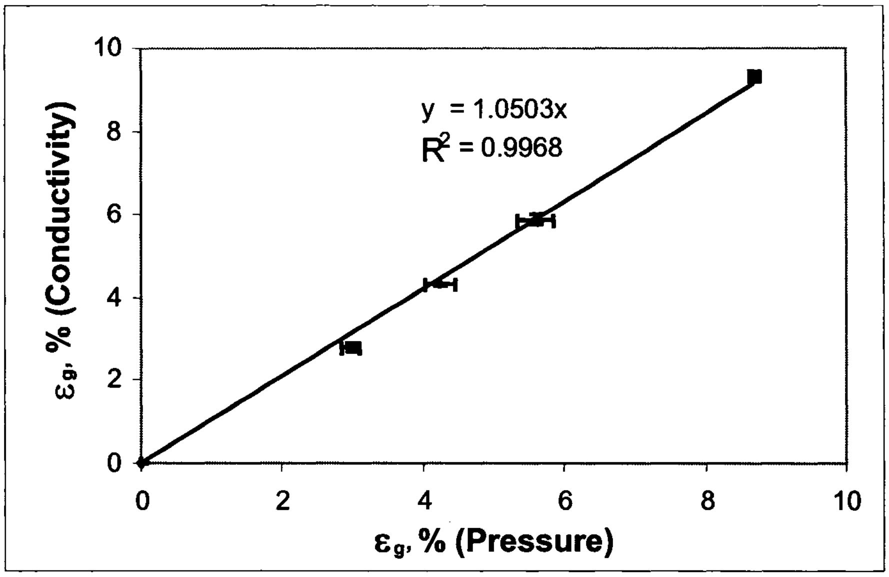

FIGURE 4.4: *Gas holdup measurements from pressure and conductivity techniques*

4.3.2 Water overflow rate (J_{wo})

The water carrying rate was measured as the water overflow rate (J_{wo}), the volumetric flowrate of water to the overflow (Q_{wo}, cm^3/s) per column cross sectional area (A, cm^2) i.e., $J_{wo} = Q_{wo}/A$. The Q_{wo} was measured at a constant foam height over a period of time after steady state had been reached.

4.4.3 Bubble size

Bubble size distribution measurements were performed on four frothers (the reason for their selection will be covered later), n-pentanol, MIBC, Dowfroth250 and F-150. One purpose of the measurements was to determine the Sauter mean diameter to calculate S_b and explore the relationship with J_{wo}. Figure 4.5 shows the McGill bubble viewer that was used [Hernandez-Aguilar et al., 2002, 2004]. The device was placed on top of the column with the sampling tube in the centre and 50cm above the sparger (to try to ensure bubbles have had time to be well dispersed).

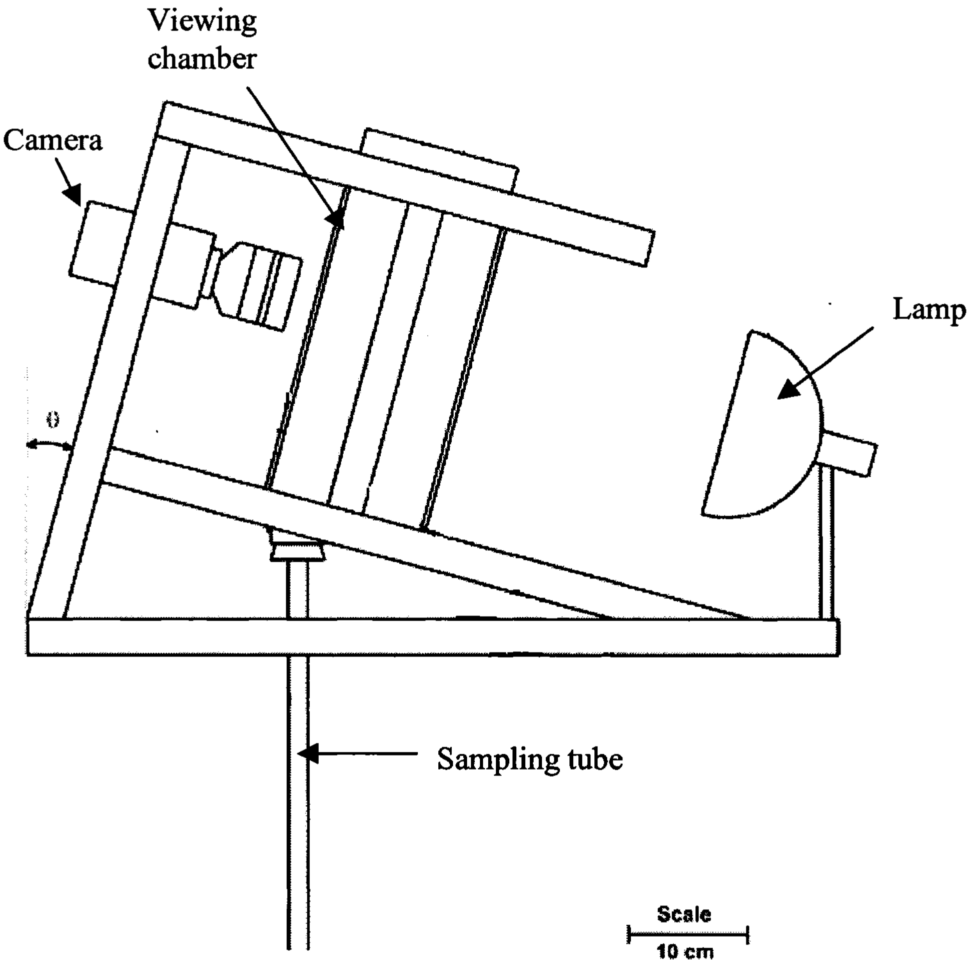

FIGURE 4.5: *McGill bubble viewer. θ is the angle of inclination of the viewing chamber 15° in this case [Hernandez, 2004].*

4.4 FROTHER COMPARISON

Table 4.1 gives a summary of the frothers examined and test conditions. The frothers were used as supplied. Salt (potassium chloride) was added to bring the conductivity of the solutions to about 0.40mS/cm to increase measurement sensitivity. For each frother, the conductivity values for the unaerated solution were obtained prior to starting the test. The height of the solution in the column was then adjusted, leaving a 25cm space at the top for foam build up. Air was introduced and the system was allowed to reach steady state before adjusting to the desired foam depth (7, 15 and 35cm). At the target foam depth (height), conductivity values were noted and water overflow was collected for 3 to 5 minutes, depending on the flow rate. The foam height was controlled constant (by automatic manipulation of the feed rate) while the water overflow was collected[1]. For any particular foam height, the gas holdup values reported in Chapter 5 are the mean value of all the cells in the collection zone.

TABLE 4.1: *Summary of frothers, suppliers and test conditions*

Frother	**Supplier**	**Concentration range**		**J_g, cm/s**
		ppm	**$*10^{-3}$ Mol/L**	
n-Pentanol	Sigma Aldrich	100-150	1.1 –1.7	1.25-2.5
n-Hexanol	Sigma Aldrich	30-80	0.29-0.78	1.0-2.5
n-Heptanol	Fischer Scientific	30-80	0.25-0.69	1.0-1.75
n-Octanol	Sigma Aldrich	30-80	0.23-0.61	0.75-1.75
MIBC	Sigma Aldrich	30-80	0.29-0.78	1.0-2.5
Ethoxylated C_6 alcohol	Minerec	20-50	0.14-0.34	0.75-2.0
Dowfroth 200	Minerec	50-100	0.25-0.5	1.0-2.0
Dowfroth 250	Minerec	50-80	0.2-0.32	0.75-1.75
F-150	Minerec	30-50	0.075-0.125	0.75-1.50

---

[1] In principle, overflow rate could be estimated from feed rate; this required a calibrated pump curve and was used occasionally as a check.

CHAPTER 5

RESULTS: WATER CARRYING RATE VS GAS HOLDUP

This chapter outlines how gas holdup was established as the independent variable and was then used to compare and classify frothers into groups based on water carrying rate.

5.1 GAS HOLDUP AS THE INDEPENDENT VARIABLE

Gas holdup was measured as a function of gas rate and frother type and concentration. Figure 5.1 shows the typical relationship for three n-hexanol concentrations: a general increase in gas holdup with gas rate and frother concentration is observed.

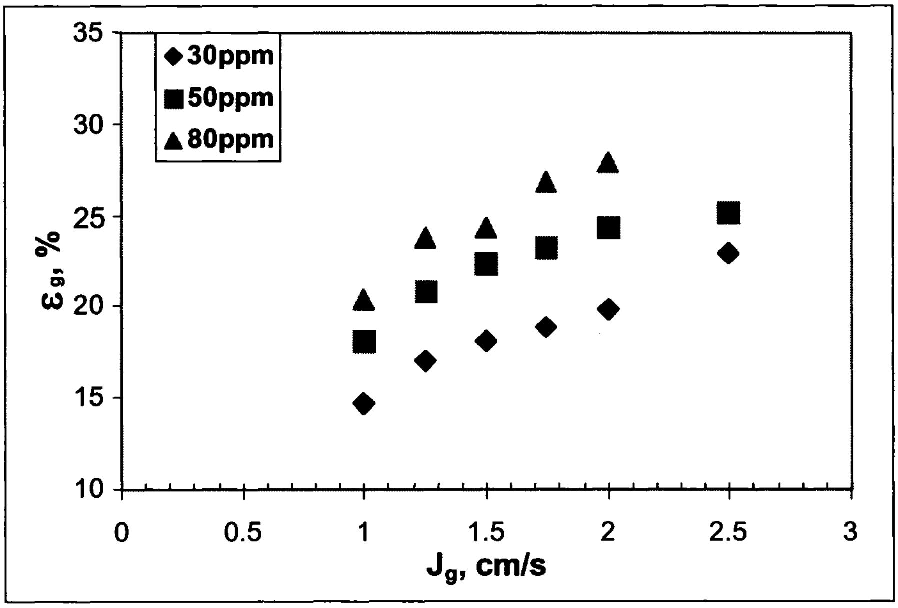

FIGURE 5.1: *Solution gas holdup as a function of gas rate and n-hexanol concentration*

The water overflow rate (water carrying rate, J_{wo}) as a function of J_g corresponding to the data in Figure 5.1 is shown in Figure 5.2. Linear trends are evident but J_{wo} is clearly not related to J_g alone.

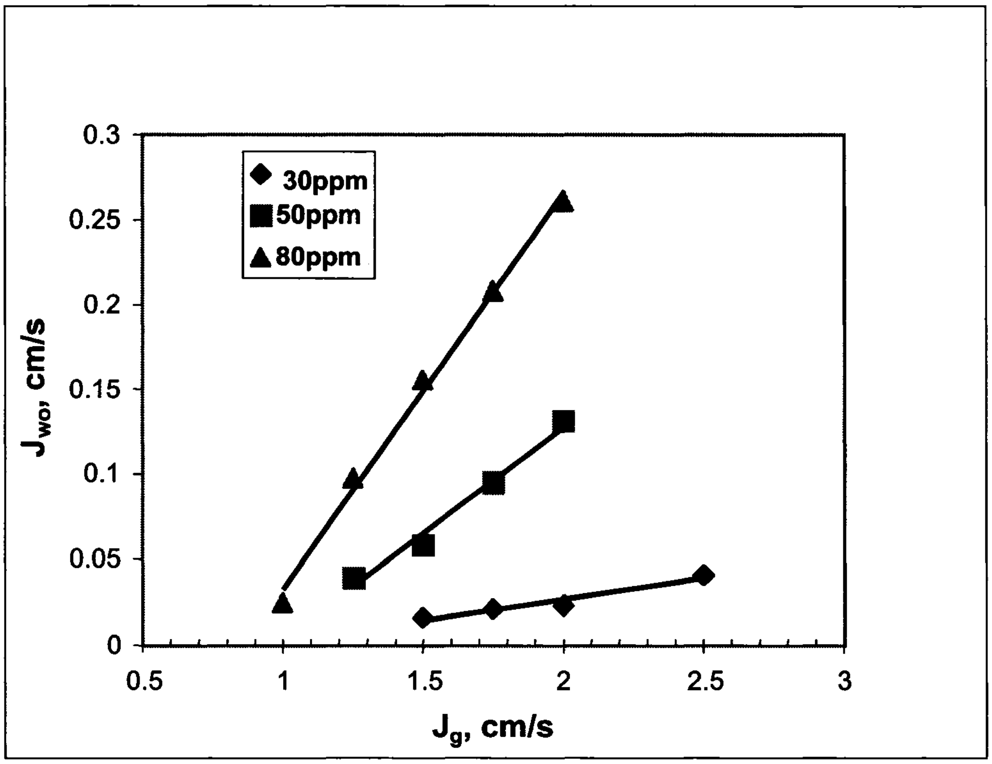

FIGURE 5.2: *J_{wo}-J_g relationship: effect of frother concentration. Conditions: n-hexanol, foam height H_f = 7cm*

There is a hint when comparing Figure 5.1 and Figure 5.2 that gas holdup could be the independent variable as both ε_g and J_{wo} increase with J_g and frother dosage. Figure 5.3 shows that plotting J_{wo} against gas holdup does collapse the data into a single trend. Above ca $\varepsilon_g = 20\%$ the trend is approximately linear (at $\varepsilon_g < 20\%$, foam could not build to the target maximum depth of 35cm).

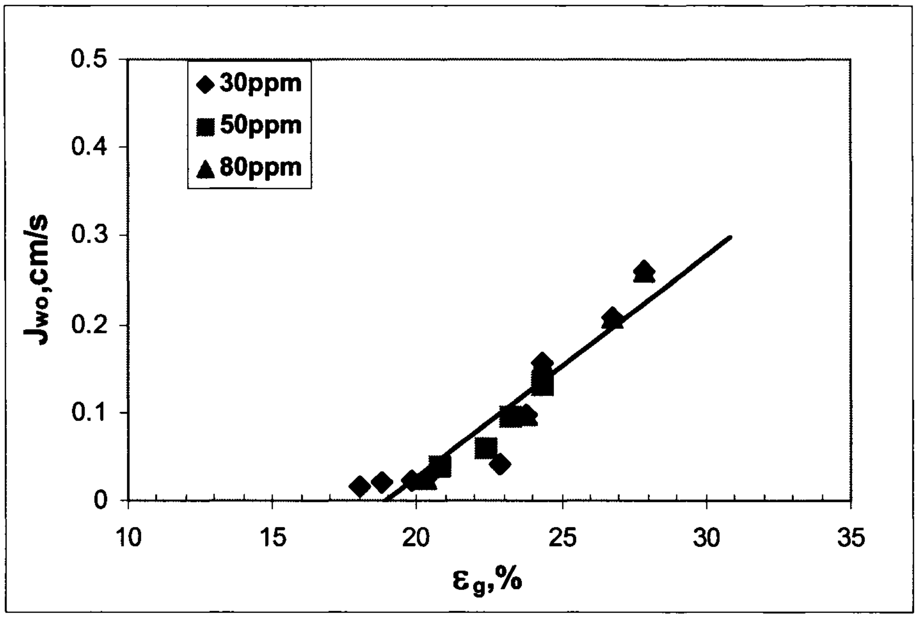

FIGURE 5.3: *J_{wo}-ε_g relationship. Conditions: n-hexanol, foam height (H_f)= 7cm*

5.1.1 Sparger Porosity

To further test the J_{wo}-ε_g relationship, two spargers of different porosities were tested. Octanol was used in this case because hexanol could not produce sufficient foam depth (i.e., 35cm) when using the coarse porosity sparger. Figure 5.4 gives the J_{wo}-J_g plot and Figure 5.5 that for J_{wo}-ε_g. Again, using the gas holdup collapses the data to a single relationship.

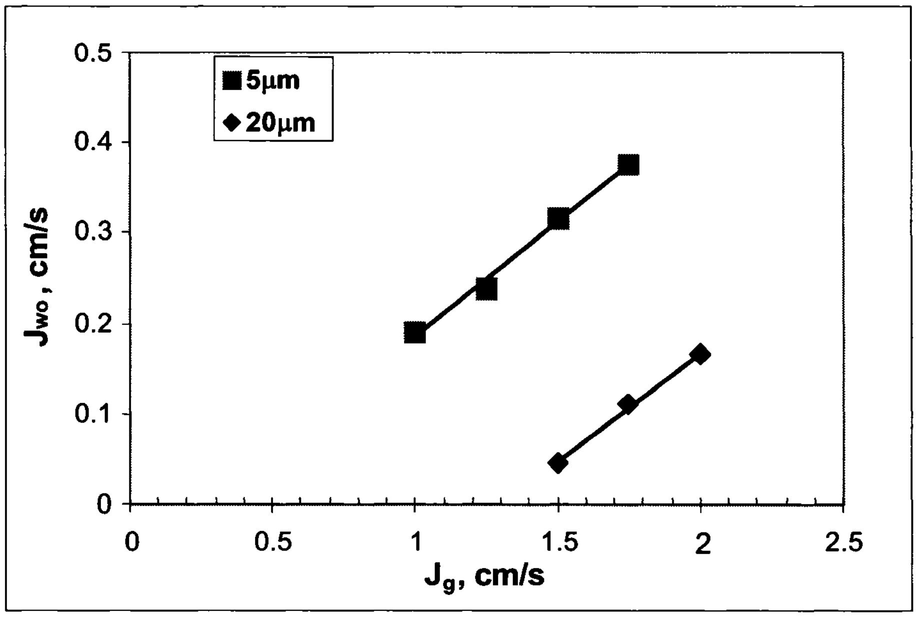

FIGURE 5.4: *J_{wo}-J_g relationship: effect of sparger porosity. Conditions: n-octanol 50ppm, foam height (H_f) 7cm*

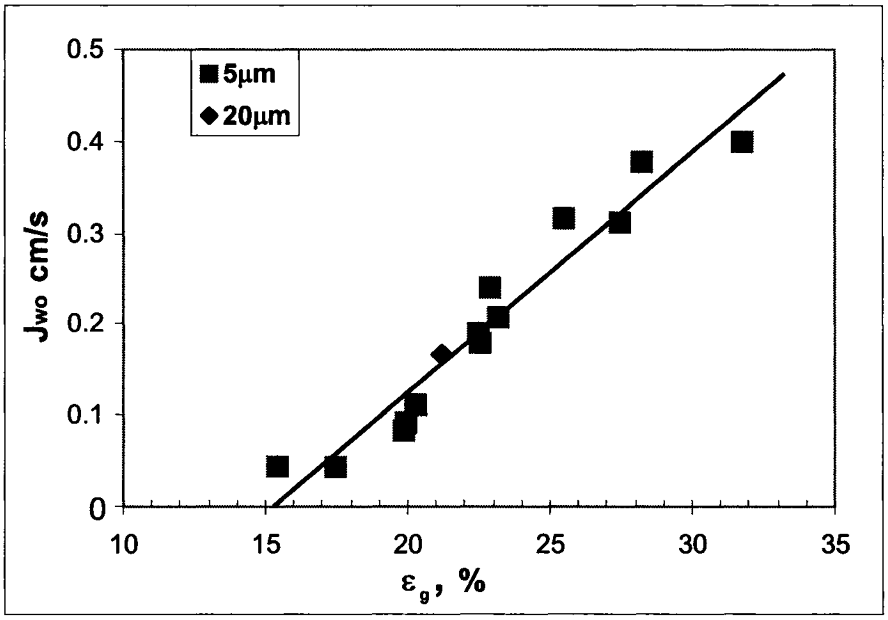

FIGURE 5.5: *J_{wo}-ε_g relationship: effect of sparger porosity. Conditions: n-octanol 50ppm, foam height (H_f) =7cm*

5.1.2 Choice of foam height

Gas holdup appears to be an appropriate independent variable. The next choice is foam height. The test conditions (sparger porosity, gas rate and frother concentration) were selected to attain at least 35cm of foam. This permitted a range in foam height to be explored. Three foam heights were tested. Figure 5.6 shows that for n-pentanol different slopes were obtained for each height while for n-octanol this was not apparent. At 7cm foam height, the two frothers had comparable slope and this proved to be the case (as will be seen) for all frothers. The 7cm foam height was then selected to compare the frothers.

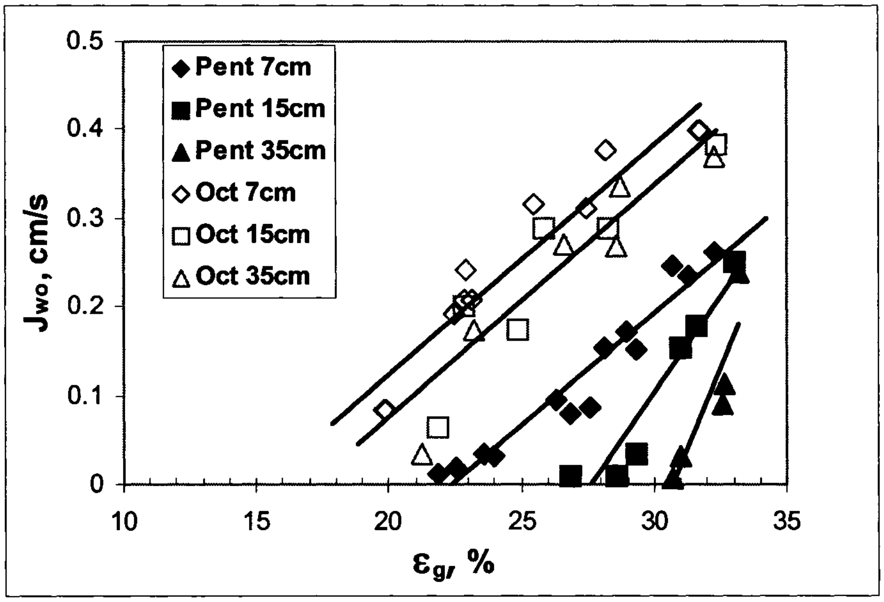

FIGURE 5.6: *J_{wo}-ε_g relationship: choice of foam height*

At any foam height some degree of water drainage must contribute to the measured J_{wo}. As height increases, drainage will increase. This complicates the concept of bubble water carrying rate (i.e., it becomes a mix of carrying and drainage rates). To minimize drainage effects, foam heights less than 7cm would be ideal, however maintaining constant a more shallow foam height proved difficult particularly when a frother generates large foam volumes. The foam height of 7cm offered a compromise with operability.

5.2 FROTHER CHARACTERIZATION

A comparison of straight chain alcohols (n-alcohols) is shown in Figure 5.7. An increase in the water overflow rate with carbon chain length (C_5-C_8) is observed. Combining all data on alcohols (Figure 5.8) they appear to classify into 3 groups (Figure 5.8). Note that the ethoxylated C_6 alcohol did not behave like the other C_6 alcohols (MIBC and n-hexanol) but rather was similar to octanol; this may be attributable to the two extra carbons in the ethoxy group that make it behave like a C_8 alcohol.

Figure 5.9 shows a comparison of polyglycol-type frothers. The two Dowfrothers show an increase in J_{wo} with chain length. The F-150 gave the highest J_{wo} of all frothers tested. Figure 5.10 shows all the frothers tested classify into four major groups.

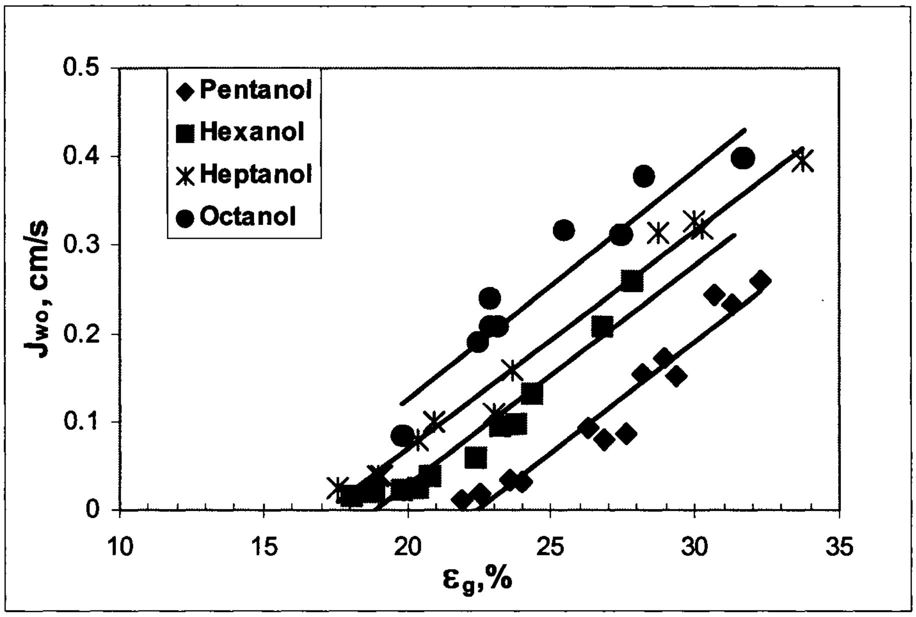

FIGURE 5.7: *J_{wo}-ε_g relationship: comparison of n-alcohols. Conditions: H_f =7cm*

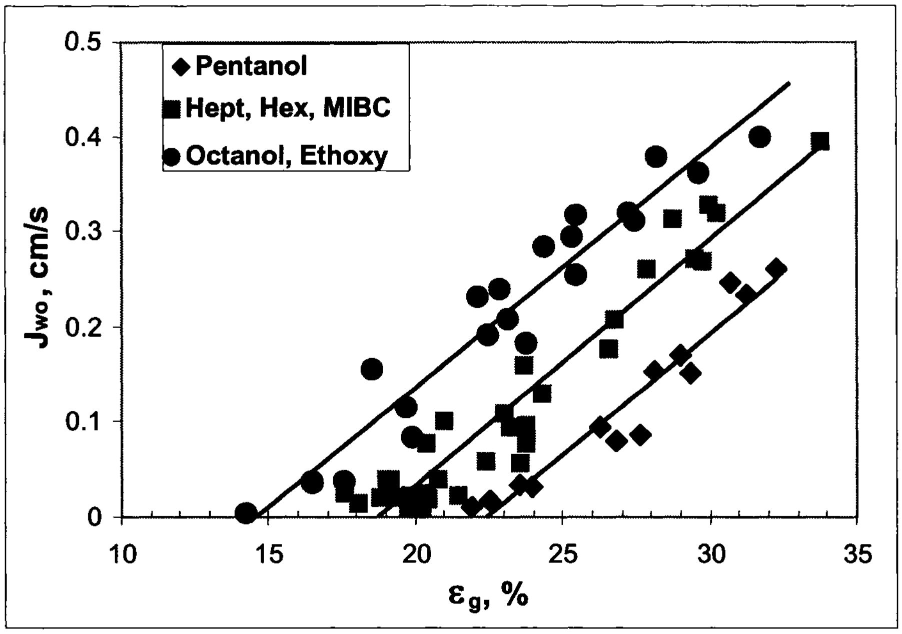

FIGURE 5.8: *J_{wo}-ε_g relationship: classification of alcohols. Conditions: H_f = 7cm*

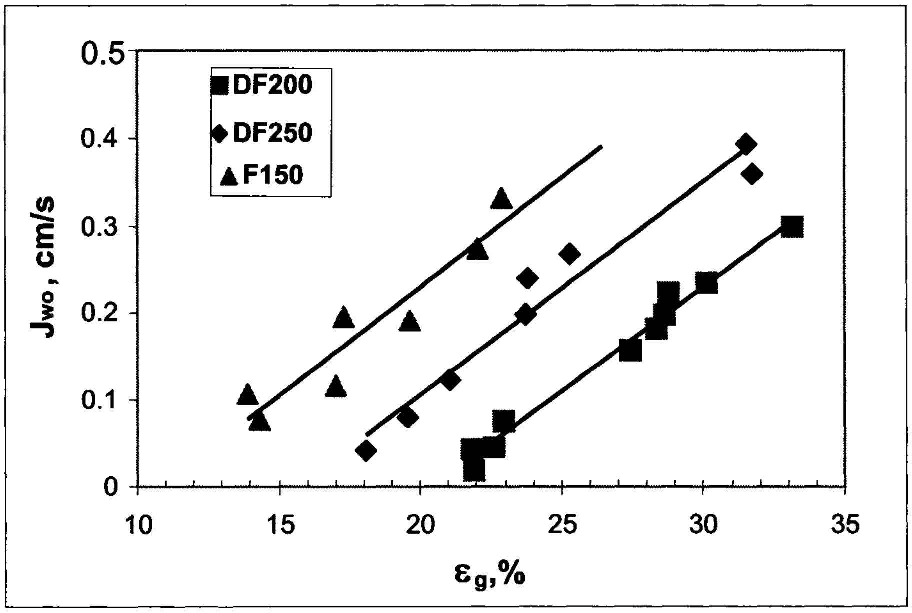

FIGURE 5.9: *J_{wo}-ε_g relationship: comparison of polyglycol type frothers. Conditions: H_f =7cm*

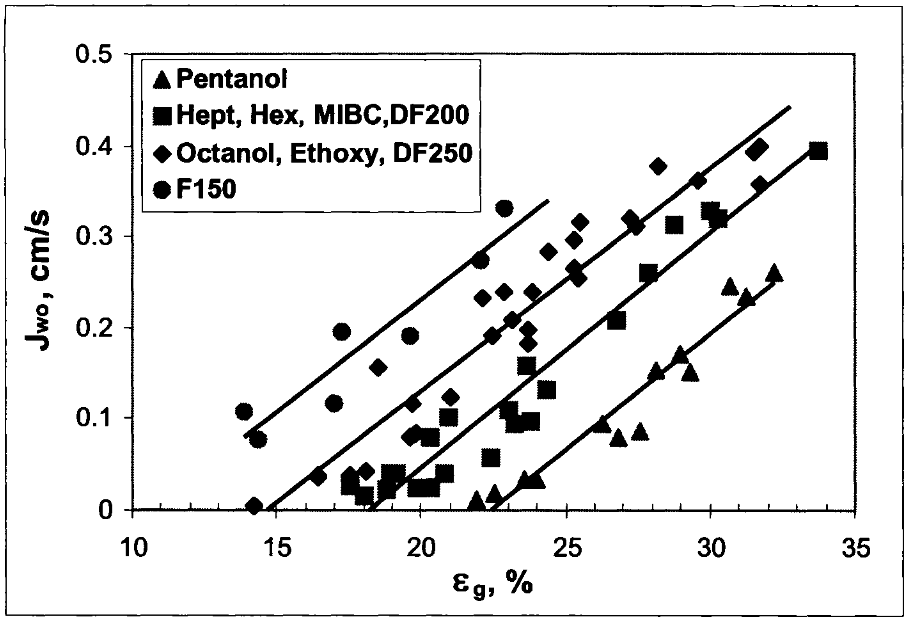

FIGURE 5.10: *J_{wo}-ε_g relationship: results for and classification of all frothers tested. Conditions: H_f =7cm*

CHAPTER 6

RESULTS: WATER CARRYING RATE VS BUBBLE SURFACE AREA FLUX

Bubble size data can reveal much about the impact of reagents in a flotation system. The information can be presented as: frequency distribution (number, surface and volume), cumulative frequency and various mean diameters, e.g., mean equivalent number spherical diameter (d_{10}) and Sauter mean diameter (d_{32}), the latter being normally used to calculate surface area flux (S_b). The S_b was another parameter that was considered as a way to correlate against the water carrying rate data and thus help isolate frother chemistry effects. According to equation 2.5, J_{wo} should be proportional to S_b, the constant being the equivalent water layer thickness (δ). In this chapter, bubble size and S_b are explored as independent variables to correlate against J_{wo}.

6.1 BUBBLE SIZE AS THE INDEPENDENT VARIABLE

Frother dosage and gas rate are the prime variables that control bubble size, outside of the bubble generation device itself. Figure 6.1 illustrates the effect of these variables on the Sauter mean bubble size (d_{32}). Increasing gas rate consistently increased the bubble size; frother addition from 30 to 50ppm, however, did not have a noticeable effect. This implies that the CCC (critical frother concentration) has been exceeded. Previous studies tend to support such a conclusion at these concentrations [Cho and Laskowski, 2002].

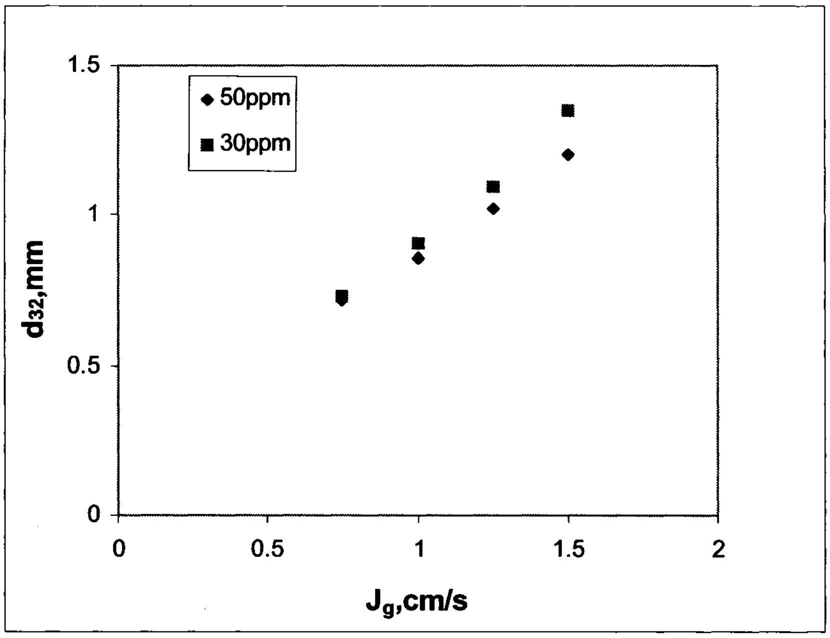

FIGURE 6.1: *Variation of bubble size with gas rate; effect of frother dosage. Frother F-150*

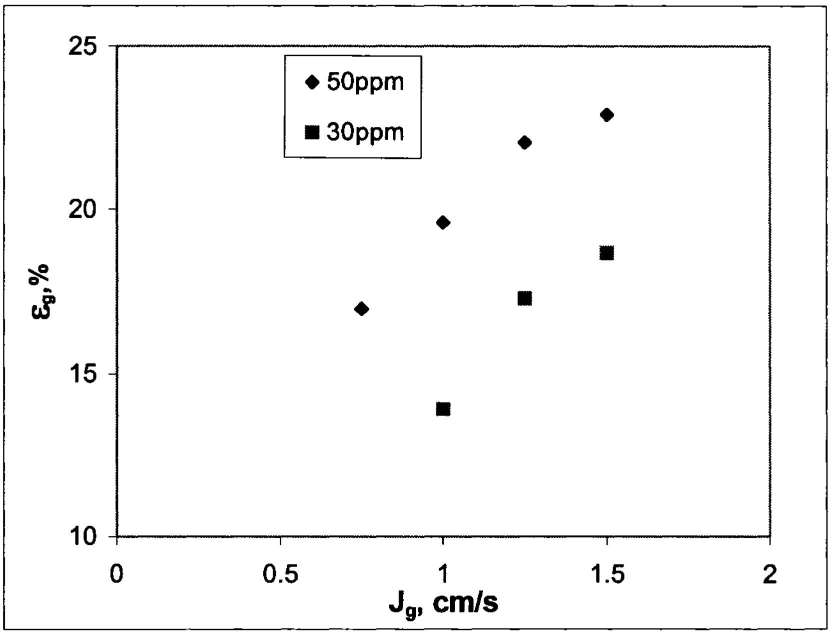

FIGURE 6.2: *ε_g-J_g relationship: effect of frother dosage. Conditions: F-150*

Since bubble size did not change much with frother dosage it might be expected that gas holdup would not change much either. Figure 5.1 clearly showed that this was not the case. Figure 6.2 re-emphasizes this point for F-150 by comparison with Figure 6.1: increasing the frother dosage from 30ppm to 50ppm had a pronounced effect on ε_g despite the minimal effect on bubble size.

Figure 6.3 shows a variation of J_{wo} with d_{32} (the increase in d_{32} is a result of gas rate). It is clear that bubble size is not an independent variable since the data still separate according to frother concentration.

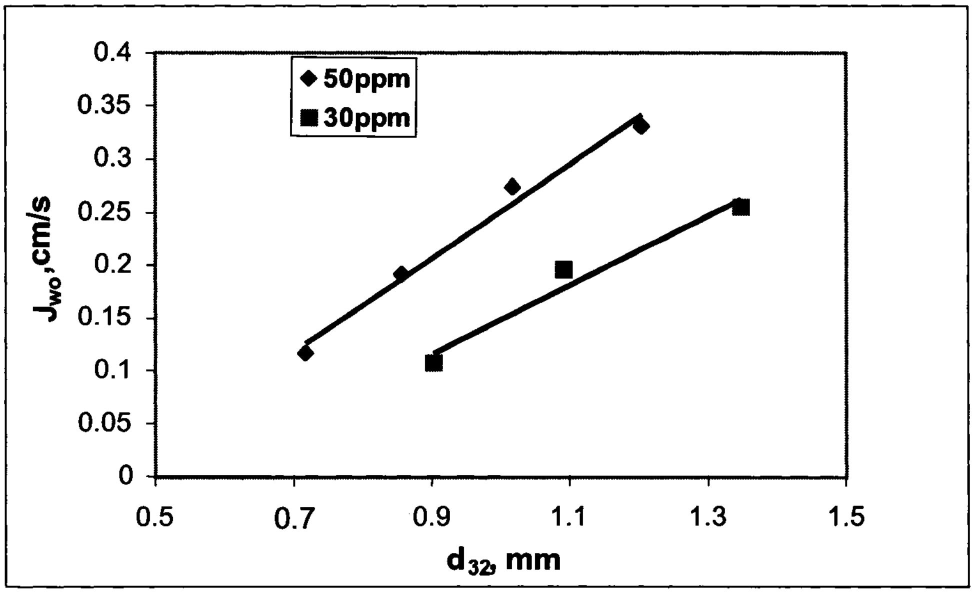

FIGURE 6.3: *J_{wo}-d_{32} relationship: Conditions: F-150, H_f = 7cm*

6.2 BUBBLE SURFACE AREA FLUX AS THE INDEPENDENT VARIABLE

Figure 6.4 gives a plot of d_{32} against J_g for four frothers, one from each of the "families" identified in Figure 5.10. There is not much difference in bubble size at low J_g, however at high J_g differences start to emerge, notably n-pentanol gives the largest bubble and F-150 the smallest. From Figure 5.10 it can be inferred that a bubble carries less water when n-pentanol is used as opposed to F-150. It follows therefore that at high J_g where bubble collision probability is high F-150 would retard coalescence much better than n-pentanol. It is supposed that F-150, a polygylcol, forms strong H-bonds with water molecules resulting in a thicker water layer that resists film drainage and rupture.

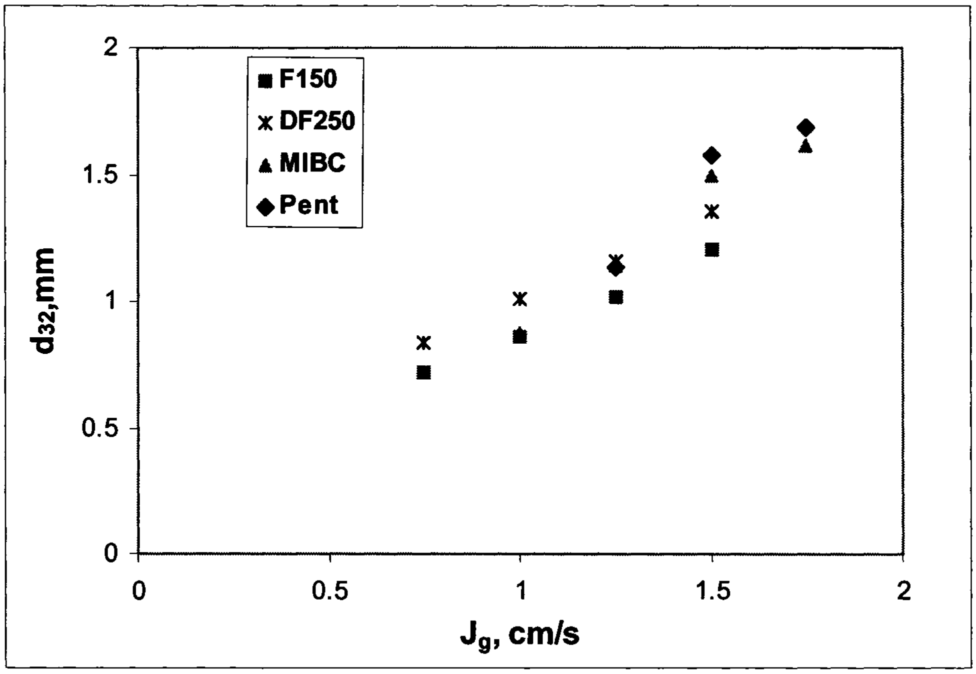

FIGURE 6.4: *d_{32}-J_g relationship: effect of frother type. Conditions: 50ppm DF250; 50ppm F-150; 80ppm MIBC; 150ppm n-pentanol.*

Figure 6.5 illustrates the influence of bubble size on J_{wo}. Again the influence of frother chemistry is demonstrated despite the small difference in bubble size. The increase in d_{32} is simply because J_g is increased (see Figure 6.4). The trend in Figure 6.5 is comparable to that in Figure 5.10 showing that even though the frothers reduce bubble size to almost the same extent the amount of water carried is strongly influenced by frother type.

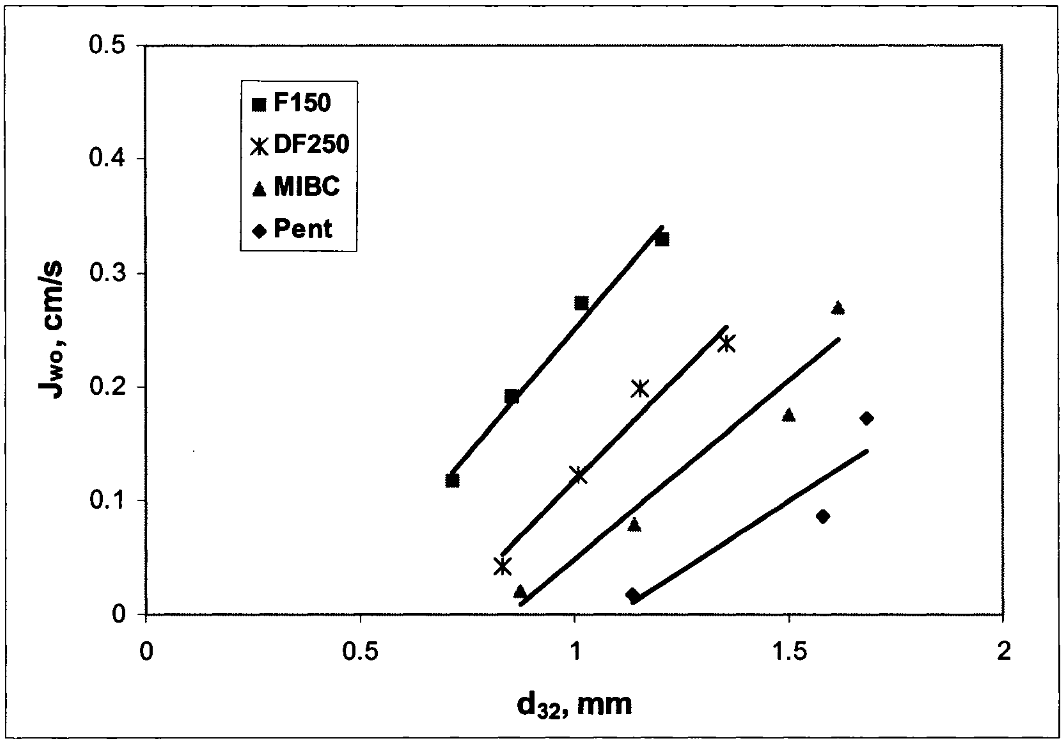

FIGURE 6.5: *J_{wo}-d_{32} relationship. Conditions: H_f = 7cm; 50ppm DF250; 50ppm F-150; 80ppm MIBC; 150ppm n-pentanol.*

Figure 6.6 gives the J_{wo}-S_b plot for the different frothers. N-pentanol and MIBC show J_{wo} continues to increase while S_b remains almost constant. From the bubble size data it was observed that at the frother dosages investigated, bubble size did not change for n-pentanol and MIBC. There was a slight bubble size reduction for DF 250 and F-150 over the concentration range in Figure 6.6 hence the trend observed between J_{wo} and S_b.

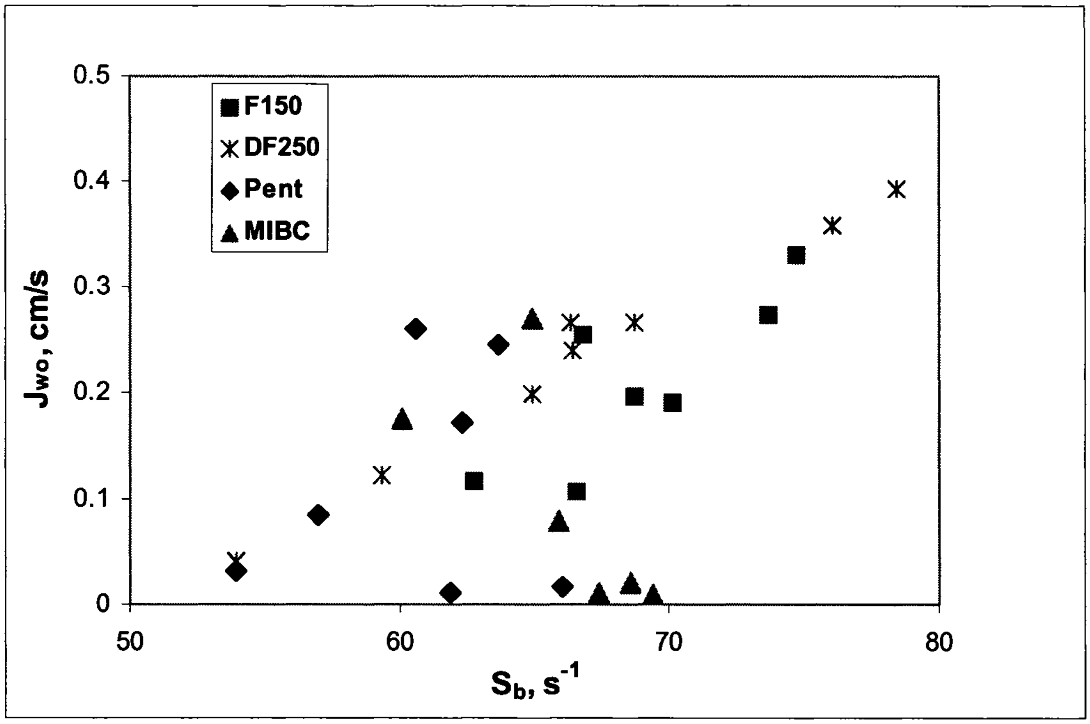

FIGURE 6.6: *J_{wo}-S_b relationship. Conditions: H_f = 7cm*

CHAPTER 7

DISCUSSION

This chapter explores the possible explanations of the trends observed in chapters 5 and 6. The points to be discussed include:

- (i) J_{wo}-ε_g relationship
  - a. Success of ε_g as the independent variable
  - b. Relevance to flotation
- (ii) J_{wo}-S_b relationship

7.1 J_{wo}-ε_g RELATIONSHIP

Figure 5.10 shows that for each frother type J_{wo} is uniquely related to ε_g; as ε_g increases J_{wo} increases linearly. The increase in ε_g is due to an increase in both frother concentration and gas rate (Figure 5.1), which concurrently results in an increase in J_{wo} (Figure 5.2). The resulting effect of both parameters (frother concentration and gas rate) on J_{wo} and ε_g is independent of frother type hence the same slope is obtained. The extent to which J_{wo} increases with gas holdup is, however, dependent on frother type which distinctively characterizes the frothers.

7.1.1 Success of ε_g as the independent variable

Gas holdup is a function of gas rate and bubble velocity i.e., the finer the bubble size the slower it rises thus the higher the gas holdup. Any change in the system that causes rise velocity to change will be reflected by a change in gas holdup. Figure 6.1 and Figure 6.4 showed that bubble size hardly reacted to changes in frother dosage and frother type, respectively, while Figure 5.1 and Figure 6.2 indicate that ε_g continued to increase with frother dosage. Possible explanations as to why gas holdup increases with frother dosage while bubble size remains constant are considered in section 7.2. The sensitivity of ε_g to such changes qualifies it as the appropriate variable to isolate frother chemistry.

7.1.2 Relevance to flotation

The J_{wo}-ε_g method of characterizing frothers offers a way of selecting and comparing frothers based on a basic function of a frother, namely transport of water. In this case, the experimental conditions chosen gave the same range of gas holdup values such that the difference between frothers is based solely on the water carrying rate characteristics of an individual frother. The hypothesis that the water carried by a bubble is influenced by frother type was validated by the J_{wo}-ε_g relationship.

7.2 J_{wo}-S_b RELATIONSHIP

Largely based on drift flux analysis, Finch et al. (2000) found that S_b was linearly related with ε_g (S_b (s^{-1})~ 5.5 ε_g (%)). It was expected therefore that the J_{wo}-S_b relationship would follow the same trend as J_{wo}-ε_g. Figure 7.1 shows for the current data that gas holdup is independent of S_b, continuing to increase while S_b is constant. The lack of frother concentration effect on bubble size because the CCC is exceeded (Figure 6.1) gives an explanation for the failure of S_b to correlate with J_{wo}; however it does not explain why ε_g changes with frother dosage. Some possible explanations are:

(i) The d_{32} is too insensitive to the change in the population of fine bubbles that influence gas holdup. Using % < 0.5mm, does reveal an increase in bubble fineness with frother dosage (Figure 7.2) but this disappears at $J_g \geq 1.25$cm/s while gas holdup remains sensitive to frother dosage.

(ii) Fine bubbles (<0.5mm) are not detected by a combination of the imaging software (detection limit is ca 0.2mm) and their failure to enter the sampling tube (there is a downward liquid velocity generated that will hinder the rise of smaller bubbles). Figure 7.2 shows a decrease in % < 0.5mm with J_g. This trend is expected since an increase in J_g increases bubble size but this could also reflect that the increase in J_g, which results in an increase in downward liquid velocity in the sampling tube, blocks fine bubble entry.

(iii) The size may be genuinely constant but the bubble slows down as a result of other factors. For instance, if the water layer carried on the bubble increases in thickness with frother dosage (as the J_{wo} results imply), this added mass could slow the bubble rise. Certainly for a given bubble size, J_{wo} does vary with concentration which suggests it is related to the boundary water layer thickness (Figure 6.3). This effect should show as a decrease in terminal velocity of a single bubble. The evidence appears contrary, Sam et al., (1996) concluded that terminal velocity is independent of frother concentration, but that work is worth repeating as the possibility that bubble size changed with dosage was not considered.

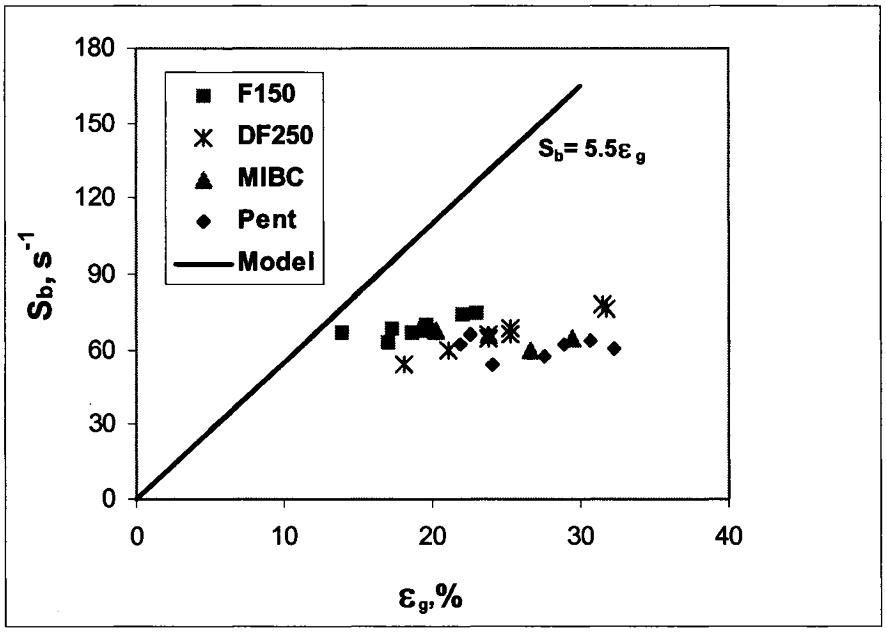

FIGURE 7.1: *S_b-ε_g relationship*

On balance, at this stage, the suspicion is that the population of fine bubbles does increase with frother dosage above the apparent CCC and this is detected by the gas holdup but not by the bubble sizing method. A simple test may be to switch the gas off and record the time for bubbles to exit the column as a function of frother dosage; the longer the time the greater the fine bubble population.

One possible way of exploring the J_{wo}-S_b relationship is to work below CCC, where frother dosage does impact bubble size. In the current set-up, frother dosages below CCC were not compatible with meeting the foam depth of 35cm. Using a downward flow of water into the foam or adding salt or some hydrophobic solids to stabilize the froth may enable work below CCC.

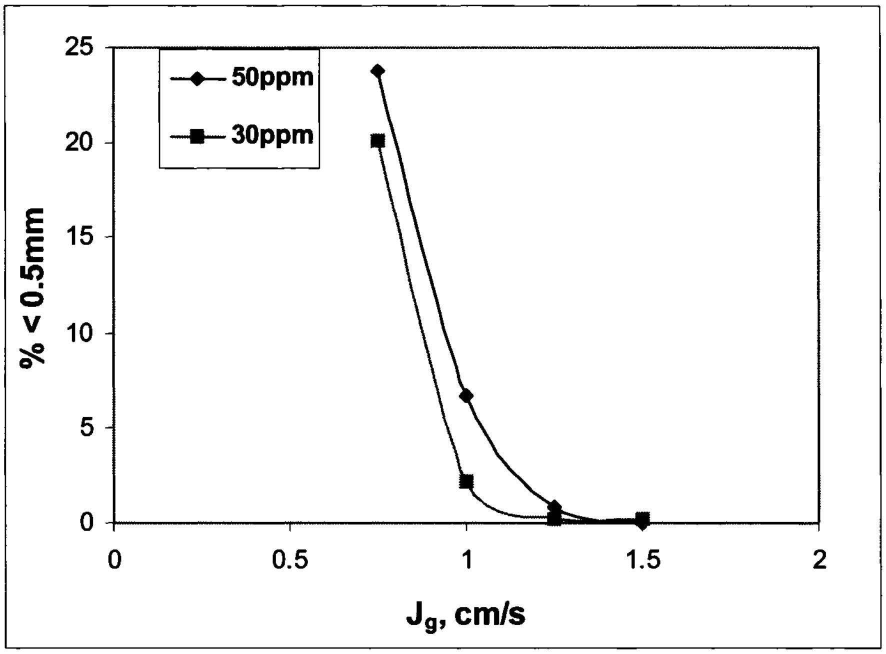

FIGURE 7.2: *Influence of J_g on % < 0.5mm*

CHAPTER 8

CONCLUSIONS AND RECOMMENDATIONS

8.1 CONCLUSIONS

The following conclusions were reached:

(i) A proposed classification of frothers based on water carrying rate is introduced.

(ii) The use of gas holdup removes gas rate and bubble size effects, and isolates frother chemistry effects.

(iii) Frothers divide into 4 groups according to the carrying rate-gas holdup (J_{wo}-ε_g) relationship

F-150>n-octanol, ethoxy C_6 alcohol, DF250

>n-heptanol, n-hexanol, MIBC, DF200>n-pentanol.

(iv) A correlation between water carrying rate and bubble surface area flux could not be established.

(v) There is a possibility that fine bubbles are produced at high frother dosages and are missed in the sampling/imaging process. This could result in the little apparent effect of high frother dosage on bubble size making the bubble surface area flux incorrect and explaining its lack of correspondence with water carrying rate.

(vi) The hypothesis that water transport is a function of frother type was validated using the J_{wo}-ε_g relationship.

8.2 FUTURE WORK

To further understand the influence of frothers on water carrying rate the following recommendations are made:

(i) The relationship between water carrying rate and bubble surface area flux may be better tested if lower frother dosages are used, i.e., range of frother dosages which causes a noticeable change in bubble size. The foam height criterion will need to be relaxed.

(ii) Investigate using hydrophobic solids to promote froth stability and permit lower frother dosages to be used. This system would also be closer to flotation

(iii) Resolve the concern over the 'missing' fine bubbles in estimation of S_b at high frother dosages.

(iv) Introduce fine hydrophilic particles e.g. fine silica < 38μm and relate silica recovery to water recovery for different frother types.

(v) Test quality of water. It will be interesting to further investigate how the quality of water influences the water carrying rate of frother, e.g., the role of dissolved salts, as in concentrator recycled water compared to the tap water.

REFERENCES

Ahmed, N., Jameson, G.J., 1985. The effect of bubble size on the rate of flotation of fine particles. International Journal of Mineral Processing 14 (3):195-215

Aldrich, C., and F eng, D, 2000. Effect of fluid properties on two-phase froth characteristics. Ind. Eng. Chem. Res., 38 (10): 4110-4112.

Asplin, R.A., Sadr-Kazemi, N., Cilliers, J.J., 1998. The effect of surfactant concentration on batch flotation mineral flux and froth structure. Minerals Engineering 11 (3):257-269.

Barbian, N., 2003. Froth stability and flotation performance. PhD thesis, UMIST, UK.

Barbian, N., Ventura-Medina, E., Cilliers J.J., 2003. Dynamic froth stability in froth flotation. Minerals Engineering 16: 1111-1116.

Bascur, O.A., Herbst, J.A., 1982. Dynamic modeling of a flotation cell with a view toward automatic control. 14th International mineral Processing Congress. Toronto, Canada October 17-23

Bikerman, J.J., 1938. The unit of foaminess. Trans. Faraday Society 34: 634-638

Bishop, J.P., White, M.E., 1976. a study of particle entrainment in flotation froths. Transactions of IMM 89: C191-C194

Booth, R.B. and Freyberger, W.L., 1962. Froths and frothing agents in Froth Flotation 50th Anniversary volume. Chapter 10: 258-276. Edited by Fuerstenau.

Cho, Y.S., Laskowski, J.S., 2002. Effect of flotation frothers on bubble size and foam stability. International. Journal of Mineral Processing 64: 69-80.

Comely, B.A., Harris, P.J., Bradshaw, D.J., Harris, M.C., 2002. Frother characterization using dynamic surface tension measurements. Int. J. Miner. Process. 64: 81-100

Cooper, M., Scott, D., Dahlke, R., Finch, J.A., Gomez, C.O., 2004. Impact of air distribution profiles on banks in a Zn cleaning circuit. CIM bulletin 97(1083)

Crozier, R.D., Klimpel, R.R., 1989. Mineral Processing and Extractive Metallurgy Review 5:257-279

Crozier, R.D., 1992. Flotation: Theory, reagents and ore testing. Chapter6: 85-100. Pergamon Press, New York.

Cutting,G.W., Devenish, M., 1975. A steady state model of both flotation structures. Society of Mining Engineering AIME annual meeting, New York, Preprint 75-B-56

Dobby, G.S., Finch, J.A., 1986. Particle collection in columns- Gas rate and bubble size effects. Canadian Metallurgical Quarterly 25 (1): 9-13

Ducker, W.A., Senden, T.J., Pashely, R.M., 1992. Measurement of forces in liquids using a force microscope. Langmuir 8: 1831-1836

Ekmekci, Z., Bradshaw, D.J., Allison, S.A., Harris, P.J., 2003. Effects of frother type and froth height on the flotation behaviour of chromite in UG2 ore. Min. Eng 16: 941-949.

Engelbrecht, J.A., Woodburn, E.T., 1975. The effects of froth height, aeration rate and gas precipitation on flotation. J. SAIMM: 125-131

Espinosa-Gomez, R., Finch, J.A., Bernert, W., 1988. Coalescence and froth collapse in the presence of fatty acids. Colloids and Surfaces 32:197-209

Finch, J.A., Dobby, G.S., 1990. Column Flotation. Pergamon Press, New York.

Finch J.A., Dobby, G.S., 1991. Column flotation: a selected review 1. International Journal of Mineral Processing 33: 343-354.

Finch, J. A., Xiao J., Hardie, C., Gomez, C. O., 2000. Gas dispersion properties: bubble surface area flux and gas holdup. Minerals Engineering, 13 (4): 365-372

Fuerstenau, D.W., 1999. Advances in Flotation Technology. Proceedings of Symposium of Advances in Flotation Technology held at the SME Annual Meeting. March 1-3:3-21. Edited by Parekh B.K. and Miller J.D. Society for Mining Metallurgy and Exploration, Littleton, Colorado

Gaudin, A.M., 1957. Flotation. Chapter 11: 327-368. McGraw-Hill, New York.

Gelinas, S., Finch J.A., Gouet-Kaplan, M., 2005. Comparative real-time characterization of frother bubble thin films. Journal of Colloids and Interface Science: *In press, corrected proof.*

George, P., Nguyen, A.V., Jameson, G.J., 2004. Assessment of true flotation and entrainment in the flotation of submicron particles by fine bubbles. Minerals Engineering 17: 847-853

Gomez, C.O., Finch, J.A., 2002. Gas dispersions in flotation machines. CIM Bulletin 95 (1066): 73-78

Gorain, B.K., Franzidis, J.-P., Mainlapig, E.V., 1995. Studies on impeller type, impeller speed and air flow rate in an industrial scale flotation cell-Part 1: Effect on bubble size distribution. Minerals Engineering 8 (6): 615-635

Gorain, B.K., Franzidis, J.P. and Manlapig, E.V., 1997. Sudies on impeller type, impeller speed and air flow rate in an industrial scale flotation cell: Effect of bubble surface area flux on flotation performance. Minerals Engineering, 10 (4):367-379.

Harris, C.C., 1976. Flotation machines in Flotation: A.M.Gaudin Memorial Volume. Vol 2, Chapter 27: 753-815

Harris, P.J., 1982. Frothing phenomena and frothers in Flotation principles. Chapter 13: 237-250. Edited by R.P. King

Hernandez-Aguilar, J.R., Rao, S.R. and Finch, J.A., 2004. The application of the McGill bubble viewer to the quantification of ore flotability 'P' at the microscale. AMIRA Project P9M Vol. 2 Flotation Module 2000-2003. Final Report August 2004: 127-140

Hernandez-Aguilar, J.R., 2004. An imaging technique for sizing bubbles in flotation systems. PhD thesis McGill University

Hunter, R.J., 1987. Foundation of Colloid Science, vol 1. Oxford Univ. Press, New York: 420

Iglesias, E., Anderez, J., Forgiarini, A., Salager, J-L., 1995. A new method to estimate the stability of short-life foams. Coll. & Surf. 98A: 167-174

Jachimska, B., Lunkenheimer, K. and Malysa, K., 1995. Effect of position of the functional group on the equilibrium and dynamic surface properties of butyl alcohols. Journal of Colloid and Interface Science 176: 31-38

Jowett, A., 1966. Gangue mineral contamination of froth. British Chemical Engineering 2(5): 330-333

Kaya, M., Laplante, A.R., 1986. Investigation of batch and continuous flotation kinetics in a modified Denver laboratory cell. Canadian Metallurgical Quarterly 25:1

Klassen, V.I., Mokrousov, V.A., 1963. An introduction to the theory of flotation – frothers and flotation froth. Chapter16-18: 353-415

Klimpel, R.R., Hansen, R.D., 1988. Frothers. Surfactant Science Series. Chapter 12: 385-409.

Laplante A.R., Kaya, M., Smith, H. W. 1989. The effect of froth on flotation kinetics-A mass transfer approach. Mineral Processing and Extractive Metallurgy Review 5:147-168

Laskowski, J.S., 1998. Frothers and flotation in Frothing in Flotation II. Chapter 1: 1-49. Edited by Laskowski, J. S. and Woodburn, E.T.

Laskowski, J.S., Cho, Y.S., Ding K., 2003. Effect of frothers on bubble size and froth stability in potash ore flotation systems. Canadian Journal of Chemical Engineering 80: 299-305

Laskowski, J.S., 2003. Fundamental properties of flotation frothers. Proceedings of the 22nd International Mineral Processing Congress (IMPC). 29 Sept-3Oct 2003, Cape Town, South Africa. Edited by Prof. L. Lorenzen and Dr. D. Bradshaw

Levich, V.G., 1962. Physicochemical hydrodynamics. Chapter8: 395-471. Translated by Scripta Technica Inc. Engelwood Cliffs, N.J.: Prentice-Hall

Lynch A.J., Johnson N.W., Mainlapig, E.V., Thorne, C.G., 1981. Mineral and coal flotation circuits and their simulation and control. Elsevier Scientific Publishing.

Malysa, K., Czubak-Pawlikowska, J. and Pomianowski, A., 1976. Frothing properties of solutions and their influence on floatability. Proceedings of 7th International Congress of Surface Active Substances, Moscow, Vol 3: 513-520

Malysa, K., Lunkenheimer, K., Miller, R., Hartenstein, C., 1981. Surface elasticity and frothability of n-octanol and n-octanoic acid solutions. Colloids and Surfaces 3: 329-338.

Malysa, E., Malysa, K., Czarnecki, J., 1987. A method of comparison of the frothing and collecting properties of frothers. Colloids and Surfaces 23 (1-2):29-39.

Malysa, K., Lunkenheimer, K., Miller, R., Hempt, C., 1985. Surface elasticity and dynamic stability of wet foams. Colloids & Surfaces 16:9-20

Malysa, K., 1992. Wet foams: Formation, properties and mechanism of stability. Adv. Coll. & Interf. Sci. 40: 37-80

Malysa, K., 1993. Water contents in flotation froths. XVIII Int. Miner. Process. Congress. Sydney, 23-28 May: 651-653

Malysa, K., 1999. Liquid contents in foams formed from solutions of n-pentanol, n-hexanol, n-pentanoic and hexanoic acids. Colloids and Surfaces A: Physicochemical and Engineering Aspects 156: 465-474

Maxwell, J.C., 1892. A Treatise of Electricity and Magnetism, 3rd Edition, Vol. 1, Part II, Chapter 9:435-449

M^{c}Laughlin, J.D., Quinn, P., Robertson, G., Agar, G.E., 1993. Frother evaluation. 18th International Mineral Processing Congress. Sydney, Australia 23-28 May:637-641.

Moys, M.H., 1978. A study of a plug flow model for flotation froth behaviour. International Journal of Mineral Processing 5: 21-38.

Neethling, S.J., Cilliers, J.J., Woodburn E.T., 2000. Prediction of water distribution in flowing foam. Chem. Eng. Sci., 55: 4021-4028

Neethling, S.J., Cilliers, J.J., 2002. The entrainment of gangue into a flotation froth. International Journal Mineral Processing 64:123-134.

Neethling, S.J., Lee, H.T., Cilliers J.J., 2003. Simple relationships for predicting the recovery of liquid from flowing foams and froths. Minerals Engineering. 16:1123-1130

Rao, S.R., 2004. Surface Chemistry Volume 2, Chapter 13:621-674

Riggs, W.F. Frothers- An operator's guide. Chemical reagents in the mineral processing industry

Rodel, K., 1981. Proof of boundary surface water and its effect on colloidal-chemical properties. IR spectroscopy of foam films. Tenside Detergents 18(3): 141-148

Ross, S., Suzin, Y., 1985. Measurement of Dynamic foam stability. Langmuir 1:145-149

Sam, A., Gomez, C.O., Finch, J.A., 1996. Axial velocity profiles of single bubbles in water/frother solutions. International Journal of Mineral Processing 47: 177-196.

Smith, P.G. and Warren L.J., 1989. Entrainment of particles into flotation froths. Frothing in flotation I: 123-145. Edited by Laskowski, J.S Gordon and Breach Science Publishers, New York.

Subrahmanyam, T.V. and Forssberg, E., 1988. Frother performance in flotation of Cu and Pb-Zn ores. Trans. Instn Min. Metall. (Sect C: Mineral Process. Extr. Metall.), 97: C134-142

Sun, S-C., 1952. Frothing characteristics of Pine oils in flotation. Trans. AIME 256: 65-71

Sutherland, K.L. and Wark, I.W., 1955. Principles of flotation. Australian Institute of Mining and Metallurgy Inc. Chapter 18:405-428

Sweet, C., van Hoogstraten, J., Harris, M., Laskowski, J.S., 1997. The effect of frothers on bubble size and frothability of aqueous solutions. Proceedings of the second UBC-Mcgill bi-annual international symposium of fundamentals of mineral processing and the environment, Sudbury, Ontario, August 17-19. Proccessing of complex ores: Mineral Processing and the environment. Edited by Finch, J.A., Rao S.R. and Holubec, I.

Trahar, W.J., 1981. A rational interpretation of the role of particle size in flotation. International Journal of Mineral Processing 8: 289-327

Trahar, W.J., and Warren, L.J., 1976. The floatability of very fine particles- a review. International Journal of Mineral Processing 3:103-123.

Wantke, K., Malysa, K., Lunknheimer, K., 1994. A relation between dynamic foam stability and surface elasticity. Colloids & Surfaces 82A: 183-191

Warren, L.J., 1985. Determination of the contributions of true flotation and entrainment in batch flotation tests. International Journal of Mineral Processing 14: 33-44

Watkins, R.C., 1973. An improved foam test for lubricating oils. Journal of the Institute of Petroleum 59 (567): 106-113

Wills, B.A., 1997. Mineral processing technology-an intoduction to the practical aspects of ore treatment and mineral recovery. 6th edition.

Wrobel, S.A., 1953. Flotation frothers, their action, composition, properties and structure. Recent development in mineral processing, IMM symposium 23-25 September: 431-454

Xu, M., Finch, J.A., Uribe-Salas, A., 1991. Maximum gas and bubble surface rates in flotation columns. International Journal of Mineral Processing 32: 233-250.

Xu, M., Finch, J.A.,1989. Effect of sparger surface area on bubble diameter in flotation columns. Canadian Metallurgical Quartely 28 (1): 1-6

Xu, Z., Zhang, R., Zhu, J., Xi, L., 1998. A study on evaluation method of flotation frother's froth stability. 15th Proceedings- Annual International Pittsburg Coal Conference: 1573-1579. ISSN: 1075-7961

Yianatos, J.B., Finch J.A., Laplante, A.R.,1986. Holdup profile and bubble size distribution of flotation froths. Canadian Metallurgical Quarterly 25 (1): 23-29

Yoon, R.H., Luttrel, H.H., 1989. The effect of bubble size on fine particle flotation. Frothing in flotation: A volume in honour of Jan Leja. Edited by J.S. Laskowski

Zhou, Z.A., Egiebor, N.O., Plitt, L.R., 1993. Frother effects on bubble motion in a swarm. Canadian Metallurgical Quarterly .32 (2):89-96

APPENDIX 1

CONDUCTIVITY THEORY

Electrical conductivity is defined as the ability of a material to conduct electricity and is the proportionality constant in Ohms'law [Maxwell, 1892] given by

$$i = -\kappa \Delta v \qquad \text{(A1.1)}$$

where i is the current density (Amps/cm^2) and Δv is the potential gradient (volt/cm) and κ is the conductivity (S/cm). In a conductivity cell with facing plate electrodes the resistance (R) of current flow is given by

$$R = \frac{pontential \quad difference}{current} = \frac{V_A - V_B}{I} = \frac{\Delta V}{I} \qquad \text{(A1.2)}$$

where ΔV is the potential differential between two plate electrodes A and B and I is the applied electric current. For an equipontential surface the current density, i (=I/A$_{\text{cell}}$) is constant, therefore

$$I = \int_{A_{cell}} i dA_{cell} = iA_{cell} \qquad \text{(A1.3)}$$

and

$$\Delta V = V_A - V_B = -\int_a^b \Delta \upsilon dL = -\Delta \upsilon (b-a) = -\Delta \upsilon L \qquad \text{(A1.4)}$$

where L is the distance between electrode A and B, respectively. Substituting equations 4.2, 4.3 and 4.4 into 4.1 and rearranging gives

$$\kappa = K * \frac{L}{A_{cell}} \qquad \text{(A1.5)}$$

where K is conductance $(= \frac{1}{R})$.

In general, all substances conduct electricity to some degree but some materials are better conductors than others, for example aqueous salt solutions compared to air. When, for example a non-conducting phase (e.g. air) is dispersed in a conducting phase (e.g. salt solution), the conductivity decreases.

APPENDIX 2

CELL CONSTANT DETERMINATION

Table A1.1 shows the average %voltage signal for each cell and the corresponding Radiometer reading. Figure A1.1 shows a plot of the Radiometer reading against cell 10 voltage signals. A 3rd polynomial fit with a zero intercept was used. The slope of the graph was then used to convert the % voltage signal to conductivity values. Table A1.2 shows the slope values obtained for each cell and Table A1.3 shows the corresponding conductivity values for each cell.

TABLE A2.1: % *Voltage signals and the corresponding conductivity value (Radiometer)*

Kradio	Cell 10	Cell 9	Cell 8	Cell 7	Cell 6	Cell 5	Cell 4	Cell 3	Cell 2	Cell 1
0.26	25.93406677	28.86447144	24.22467	25.95442	38.779	37.53358	30.08547	44.07815	34.18804	32.5519
0.34	34.67643738	38.80472769	31.72161	34.69754	52.75476	50.5123	38.7292	61.39779	44.49102	41.5873
0.41	41.61172485	46.98299154	37.0937	40.77168	64.24941	60.46447	44.49394	76.00635	52.30509	49.01099
0.52	51.90929822	59.38287571	45.29915	50.69039	82.27822	76.0771	53.41968	101.0668	63.48335	59.26339
0.59	58.85167128	68.29649642	50.626	57.20854	95.50243	87.35288	59.25182	105.0326	71.81003	66.80797

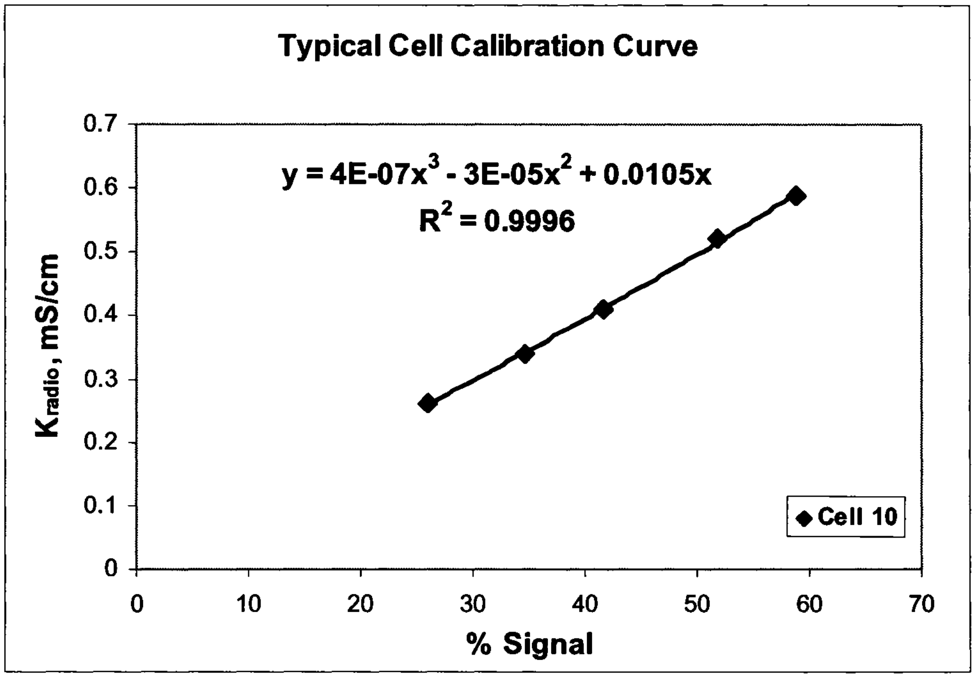

FIGURE A2.1: *Radiometer reading against cell 10 signals*

TABLE A2.2: *Slope values for each cell*

	a	b	c
Cell 10	4.30224E-07	-3.31987E-05	0.010516
Cell 9	1.0593E-07	-1.69616E-05	0.009327
Cell 8	5.95121E-07	-4.6422E-06	0.010397
Cell 7	3.39814E-07	-1.41155E-05	0.010038
Cell 6	3.88814E-08	-1.298E-05	0.007079
Cell 5	2.49787E-08	-4.49193E-06	0.006977
Cell 4	3.20404E-07	2.09389E-05	0.007628
Cell 3	1.1747E-07	-2.98364E-05	0.006963
Cell 2	-3.73889E-08	2.35374E-05	0.006755
Cell 1	-1.71763E-07	4.43223E-05	0.006668

TABLE A2.3: *Calculated conductivity values for each cell*

Kradio	Cell 10	Cell 9	Cell 8	Cell 7	Cell 6	Cell 5	Cell 4	Cell 3	Cell 2	Cell 1
0.26	0.257894376	0.257630004	0.257604	0.256964	0.257279	0.256879	0.257165	0.25901	0.256947	0.258091
0.34	0.3426713	0.342574211	0.34414	0.345497	0.343054	0.344203	0.34544	0.342231	0.343822	0.341599
0.41	0.411096571	0.411747652	0.409656	0.408835	0.411576	0.410984	0.409068	0.408452	0.41235	0.413042
0.52	0.516591045	0.51622431	0.516776	0.516823	0.516263	0.515821	0.516072	0.52024	0.514105	0.515075
0.59	0.591585384	0.591619682	0.591689	0.591689	0.591577	0.591869	0.592125	0.538311	0.592586	0.592072

Conductivity measurement VBA code

Written by Rodrigo A. Araya Ledezma

```
Option Explicit

Public dbSetPoint As Double
Dim y(10) As Double
Dim x(10) As Double
Dim vecCellConst(10, 4) As Double
Dim i As Integer
Dim x2 As Double, x3 As Double
Dim dbCriteriaLevel As Double
Dim dbHeight As Double
Dim dbX As Double


Sub LevelControlApp()

Rem This procedure calculates the conductivity from signal (0-10 volts), and then it
Rem loads the values in iFIX 3.5 database.


Err = 0
```

```
On Error GoTo Line1

Rem check for set point value
dbSetPoint = Fix32.FIX1.LEVELSETPOINT.F_CV

If dbSetPoint = 0 Then
   MsgBox "You Must Enter A Set Point Value"
End If

Rem clening up the conductivity vector
For i = 1 To 10
   y(i) = 0
Next

Rem Loading opto22 signal vector
x(1) = Fix32.FIX1.OP2MOD02.F_CV
x(2) = Fix32.FIX1.OP2MOD03.F_CV
x(3) = Fix32.FIX1.OP2MOD04.F_CV
x(4) = Fix32.FIX1.OP2MOD05.F_CV
x(5) = Fix32.FIX1.OP2MOD06.F_CV
x(6) = Fix32.FIX1.OP2MOD07.F_CV
x(7) = Fix32.FIX1.OP2MOD08.F_CV
x(8) = Fix32.FIX1.OP2MOD09.F_CV
x(9) = Fix32.FIX1.OP2MOD10.F_CV
x(10) = Fix32.FIX1.OP2MOD11.F_CV

Rem Cell Constants from calibration curve (signal v/s conductivity, polinomy order3)
Rem cell1
vecCellConst(1, 1) = -0.000000171763
vecCellConst(1, 2) = 0.0000443223
vecCellConst(1, 3) = 0.006668

Rem cell2
vecCellConst(2, 1) = 0.0000000373889
vecCellConst(2, 2) = 0.000023574
vecCellConst(2, 3) = 0.006755

Rem cell3
vecCellConst(3, 1) = 0.00000011747
vecCellConst(3, 2) = -0.0000298364
vecCellConst(3, 3) = 0.006963

Rem cell4
vecCellConst(4, 1) = 0.000000320404
vecCellConst(4, 2) = 0.0000209389
vecCellConst(4, 3) = 0.007628
```

```
Rem cell5
vecCellConst(5, 1) = 0.0000000249787
vecCellConst(5, 2) = -0.000004.49193
vecCellConst(5, 3) = 0.006977

Rem cell6
vecCellConst(6, 1) = 0.0000000388814
vecCellConst(6, 2) = -0.00001298
vecCellConst(6, 3) = 0.007079

Rem cell7
vecCellConst(7, 1) = 0.000000339814
vecCellConst(7, 2) = -0.0000141155
vecCellConst(7, 3) = 0.010038

Rem cell8
vecCellConst(8, 1) = 0.000000595121
vecCellConst(8, 2) = -0.0000046422
vecCellConst(8, 3) = 0.010397

Rem cell9
vecCellConst(9, 1) = 0.00000010593
vecCellConst(9, 2) = -0.0000169616
vecCellConst(9, 3) = 0.009327

Rem cell10
vecCellConst(10, 1) = 0.000000430224
vecCellConst(10, 2) = -0.0000331987
vecCellConst(10, 3) = 0.010516


Rem Conductivity calculation
For i = 1 To 10
   x2 = x(i) * x(i)
   x3 = x(i) * x(i) * x(i)

   y(i) = vecCellConst(i, 1) * x3 + vecCellConst(i, 2) * x2 + vecCellConst(i, 3) * x(i)

Next

Rem Eliminates noisewhen cell 3 is empty
If Abs(y(3) - y(4)) > 0.03 Then y(3) = y(2)


Rem Loading conductivity values into iFIX database
```

```
Fix32.FIX2.CONDUCTIVITY01.F_CV = y(1)
Fix32.FIX2.CONDUCTIVITY02.F_CV = y(2)
Fix32.FIX2.CONDUCTIVITY03.F_CV = y(3)
Fix32.FIX2.CONDUCTIVITY04.F_CV = y(4)
Fix32.FIX2.CONDUCTIVITY05.F_CV = y(5)
Fix32.FIX2.CONDUCTIVITY06.F_CV = y(6)
Fix32.FIX2.CONDUCTIVITY07.F_CV = y(7)
Fix32.FIX2.CONDUCTIVITY08.F_CV = y(8)
Fix32.FIX2.CONDUCTIVITY09.F_CV = y(9)
Fix32.FIX2.CONDUCTIVITY10.F_CV = y(10)

Rem Calling procedure for detecting the cell containing the interface
Call DetectLevel

Rem height results
Fix32.FIX1.LEVELMEASURE.F_CV = dbHeight
Exit Sub

Rem Error Handler
Line1:
LevelControl.tmLevelDetect.TimerEnabled = False
MsgBox "Error: " & Err & " " & Error(Err) & "--Timer Disabled", vbCritical

End Sub

Rem procedure for detecting the cell containing the interface

Sub DetectLevel()
Dim vecDifConductivity(10) As Double

Rem Loading vector used in criteria
vecDifConductivity(1) = Abs(y(9) - y(10))
vecDifConductivity(2) = Abs(y(8) - y(9))
vecDifConductivity(3) = Abs(y(7) - y(8))
vecDifConductivity(4) = Abs(y(6) - y(7))
vecDifConductivity(5) = Abs(y(5) - y(6))
vecDifConductivity(6) = Abs(y(4) - y(5))
vecDifConductivity(7) = Abs(y(3) - y(4))
vecDifConductivity(8) = Abs(y(2) - y(3))
vecDifConductivity(9) = Abs(y(1) - y(2))


dbHeight = 0
If vecDifConductivity(1) > 0.1 Then
   LevelControl.Interfacelocation.Caption = "Interface Between Rings 9-10"
   i = 9
```

```
    dbCriteriaLevel = y(i) / y(i + 1)

    Select Case dbCriteriaLevel
        Case Is < 0.3
            dbHeight = 10

        Case 0.3 To 0.59
            dbX = ((y(i + 1) - y(i)) / 2) + y(i)
            dbHeight = (10 / (y(i + 1) - y(i)) * (dbX - y(i)) + 10)

        Case Is > 0.59
            dbHeight = 20

    End Select
End If

If vecDifConductivity(2) > 0.1 Then
    LevelControl.Interfacelocation.Caption = "Interface Between Rings 8-9"
    i = 8
    dbCriteriaLevel = y(i) / y(i + 1)

    Select Case dbCriteriaLevel
        Case Is < 0.3
            dbHeight = 20

        Case 0.3 To 0.59
            dbX = ((y(i + 1) - y(i)) / 2) + y(i)
            dbHeight = (10 / (y(i + 1) - y(i)) * (dbX - y(i)) + 20)

        Case Is > 0.59
            dbHeight = 30

    End Select
End If

If vecDifConductivity(3) > 0.1 Then
    LevelControl.Interfacelocation.Caption = "Interface Between Rings 7-8"
    i = 7
    dbCriteriaLevel = y(i) / y(i + 1)

    Select Case dbCriteriaLevel
        Case Is < 0.3
            dbHeight = 30

        Case 0.3 To 0.59
            dbX = ((y(i + 1) - y(i)) / 2) + y(i)
```

```
        dbHeight = (10 / (y(i + 1) - y(i)) * (dbX - y(i)) + 30)

      Case Is > 0.59
        dbHeight = 40

    End Select
End If

If vecDifConductivity(4) > 0.1 Then
    LevelControl.Interfacelocation.Caption = "Interface Between Rings 6-7"
    i = 6
    dbCriteriaLevel = y(i) / y(i + 1)

    Select Case dbCriteriaLevel
      Case Is < 0.3
        dbHeight = 40

      Case 0.3 To 0.59
        dbX = ((y(i + 1) - y(i)) / 2) + y(i)
        dbHeight = (10 / (y(i + 1) - y(i)) * (dbX - y(i)) + 40)

      Case Is > 0.59
        dbHeight = 50

    End Select
End If

If vecDifConductivity(5) > 0.1 Then
    LevelControl.Interfacelocation.Caption = "Interface Between Rings 5-6"
    i = 5
    dbCriteriaLevel = y(i) / y(i + 1)

    Select Case dbCriteriaLevel
      Case Is < 0.3
        dbHeight = 50

      Case 0.3 To 0.59
        dbX = ((y(i + 1) - y(i)) / 2) + y(i)
        dbHeight = (10 / (y(i + 1) - y(i)) * (dbX - y(i)) + 50)

      Case Is > 0.59
        dbHeight = 60

    End Select
End If
```

```
If vecDifConductivity(6) > 0.1 Then
   LevelControl.Interfacelocation.Caption = "Interface Between Rings 4-5"
   i = 4
   dbCriteriaLevel = y(i) / y(i + 1)

   Select Case dbCriteriaLevel
      Case Is < 0.3
         dbHeight = 60

      Case 0.3 To 0.59
         dbX = ((y(i + 1) - y(i)) / 2) + y(i)
         dbHeight = (10 / (y(i + 1) - y(i)) * (dbX - y(i)) + 60)

      Case Is > 0.59
         dbHeight = 70

   End Select
End If

If vecDifConductivity(7) > 0.1 Then
   LevelControl.Interfacelocation.Caption = "Interface Between Rings 3-4"
   i = 3
   dbCriteriaLevel = y(i) / y(i + 1)

   Select Case dbCriteriaLevel
      Case Is < 0.3
         dbHeight = 70

      Case 0.3 To 0.59
         dbX = ((y(i + 1) - y(i)) / 2) + y(i)
         dbHeight = (10 / (y(i + 1) - y(i)) * (dbX - y(i)) + 70)

      Case Is > 0.59
         dbHeight = 80

   End Select
End If

If vecDifConductivity(8) > 0.1 Then
   LevelControl.Interfacelocation.Caption = "Interface Between Rings 2-3"
   i = 2
   dbCriteriaLevel = y(i) / y(i + 1)

   Select Case dbCriteriaLevel
      Case Is < 0.3
         dbHeight = 80
```

```
        Case 0.3 To 0.59
            dbX = ((y(i + 1) - y(i)) / 2) + y(i)
            dbHeight = (10 / (y(i + 1) - y(i)) * (dbX - y(i)) + 80)

        Case Is > 0.59
            dbHeight = 90

    End Select
End If

If vecDifConductivity(9) > 0.1 Then
    LevelControl.Interfacelocation.Caption = "Interface Between Rings 1-2"
    i = 1
    dbCriteriaLevel = y(i) / y(i + 1)

    Select Case dbCriteriaLevel
        Case Is < 0.3
            dbHeight = 90

        Case 0.3 To 0.59
            dbX = ((y(i + 1) - y(i)) / 2) + y(i)

            dbHeight = (10 / (y(i + 1) - y(i)) * (dbX - y(i)) + 90)

        Case Is > 0.59
            dbHeight = 100

    End Select
Else



    If dbHeight = 0 Then
        LevelControl.Interfacelocation.Caption = "Interface over ring 1"
        dbHeight = 100
    End If

End If

End Sub
```

APPENDIX 3

RAW DATA

A3.1 J_{wo}-ε_g DATA

PENTANOL

TABLE A3.1: *n-pentanol 100ppm*

J_g	Froth Height, cm	Weight/g	Time/s	Rate, g/s	ε_g	Pump speed	J_{wo}, cm/s
1					16.06399		
1.25					19.26699		
1.5	7	247	300.41	0.82221	21.89088	0.4	0.010469
1.75	7	754	300.41	2.509903	23.9959	0.7	0.031957
2	7	1892.5	301.38	6.279448	26.83209	1.2	0.079952
2	15	288.5	370.38	0.77893		0.45	0.009918
2.5	15	1062	388.5	2.733591		0.72	0.034805
2.5	7	3558	300.43	11.84302	29.34156	1.7	0.15079

TABLE A3.2: *n-pentanol 120ppm*

J_g	Froth Height, cm	Weight/g	Time/s	Rate, g/s	ε_g	Pump speed	J_{wo}, cm/s
1	5				15.7907		
1.25	7				19.55892		
1.5	7	750.5	300.34	2.498835	23.3	0.7	0.031816
1.75	7	2631	360.43	7.299614	25.83437	1.3	0.092942
2	7	3572.5	300.35	11.89446	28.13092	1.7	0.151445
2	15	1203	300.72	4.000399	27.81106	0.9	0.050935
2.5	50	845.5	301.12	2.807851	32.86515	0.74	0.035751
2.5	35	2076	300.63	6.905498	32.81403	1.28	0.087924
2.5	15	2341	180.81	12.94729	31.74865	1.8	0.16485
2.5	7	5554.5	300.41	18.48973	31.09394	3.12	0.235419

TABLE A3.3: *n-pentanol 120ppm (repeat)*

J_g	Froth Height, cm	Weight/g	Time/s	Rate, g/s	ε_g	Pump speed	J_{wo}, cm/s
1	5				16.31795		
1.25	7				20.30861		
1.5	7	809.5	301.59	2.684108	23.85789	0.7	0.034175
1.75	7	2233.5	300.25	7.438801	26.74782	1.3	0.094714
2	7	4075	330.47	12.33092	28.15333	1.7	0.157002
2	15	1689	480.4	3.51582	28.21917	0.88	0.044765
2.5	50	685	300.38	2.280445	31.56976	0.68	0.029036
2.5	35	2188	300.32	7.285562	32.40113	1.3	0.092763
2.5	15	3867	300.85	12.85358	31.98546	1.75	0.163657
2.5	7	5489	300.38	18.27352	31.47188	3	0.232666

TABLE A3.4: *n-pentanol 150ppm*

J_g	Froth Height, cm	Weight/g	Time/s	Rate, g/s	ε_g	Pump speed	J_{wo}, cm/s
1	5				17.4492		
1.25	7	406	300.44	1.351351	22.53226	0.5	0.017206
1.5	7	2025	300.34	6.742359	27.62157	1.3	0.085846
1.75	7	4099	305	13.43934	28.97217	1.86	0.171115
1.75	15	1793.5	300.41	5.970174		1.2	0.076015
1.75	35	189	331.97	0.569329	30.70238	0.9	0.007249
2	7	3476.5	180.34	19.27748	30.71528	3.2	0.245448
2	15	5634	405.68	13.88779	31.5999	1.9	0.176825
2	35	2642.5	300.31	8.799241	32.69455	1.5	0.112035
2.25	7	6158	300.57	20.48774	32.25206	3.46	0.260858
2.25	15	5122.5	260.78	19.64299	33.03653	2.68	0.250102
2.25	35	2252.5	120.25	18.73181	33.19054	2.2	0.238501

HEXANOL

TABLE A3.5: *n-hexanol 30ppm*

J_g	Froth Height, cm	Weight/g	Time/s	Rate, g/s	ε_g	Pump speed	J_{wo}, cm/s
1.0					14.69631		
1.3					16.95484		
1.5	7	371	300.37	1.235143	18.05994	0.3-0.5	0.015726
1.8	7	297	180.31	1.647163	18.81706	0.4	0.020972
2.0	7	673	370.32	1.817347	19.843	0.5	0.023139
2.5	7	672	210.13	3.19802	22.89495	0.57	0.040718

TABLE A3.6: *n-hexanol 50ppm*

J_g	Froth Height, cm	Weight/g	Time/s	Rate, g/s	ε_g	Pump speed	J_{wo}, cm/s
1	7				17.45512		
1.25	7	985	320.34	3.074858	20.76779	0.75	0.03915
1.5	7	1287.5	300.41	4.285809	22.53614	0.96	0.054569
1.5	15	340	311.79	1.090478	23.2234	0.3	0.013884
1.75	7	2229	303.25	7.350371	23.90087	1.29	0.093588
1.75	15	745.5	301.12	2.475757	23.96911	0.75	0.031522
2	7	2226.5	210.57	10.57368	25.10716	1.54	0.134628
2	15	1287.5	300.31	4.287237	25.22146	1	0.054587
2	35	526.5	330.59	1.592607	25.60538	0.5	0.020278

TABLE A3.7: *n-hexanol 50ppm (repeat)*

J_g	Froth Height, cm	Weight/g	Time/s	Rate, g/s	ε_g	Pump speed	J_{wo}, cm/s
1	7				17.45512		
1.25	7	922.5	300.62	3.068658	20.76779	0.7	0.039071
1.5	7	1741	359.78	4.839068	22.53614	0.94	0.061613
1.5	15	202	300.69	0.671788	23.2234	0.34	0.008553
1.75	7	2395.5	315.91	7.582856	23.90087	1.2	0.096548
1.75	15	808.5	302.81	2.669991	23.96911	0.65	0.033995
2	7	2420.5	241.44	10.02527	25.10716	1.3	0.127646
2	15	814.5	303.81	2.680952	25.22146	0.9	0.034135
2	35	121.5	361	0.336565	25.60538	0.37	0.004285
2.5	7	3770.5	330.4	11.41192	25.60538	1.5	0.145301

TABLE A3.8: *n-hexanol 80ppm*

J_g	Froth Height, cm	Weight/g	Time/s	Rate, g/s	ε_g	Pump speed	J_{wo}, cm/s
1	7	573.5	300.37	1.909312	20.35287	0.54	0.02431
1.25	7	2304.5	300.72	7.663275	23.77621	1.2	0.097572
1.25	15	773	359.78	2.148535	24.70504	0.64	0.027356
1.5	7	4038.5	330.53	12.21826	24.32425	1.6	0.155568
1.5	15	1811.5	300.74	6.023475	24.70424	1.06	0.076693
1.5	35	940	320.35	2.934291	27.3823	0.66	0.037361
1.75	7	4915.5	300.71	16.34631	26.75977	1.9	0.208128
1.75	15	3510	315.5	11.1252	27.38815	1.48	0.14165
1.75	35	1885	315.72	5.97048	27.70148	1.05	0.076019
2	7	6166.5	300.75	20.50374	27.85994	2.76	0.261062
2	15	4588.5	300.37	15.27616	28.87686	1.8	0.194502
2	35	3437	315.5	10.89382	28.97446	1.45	0.138704

MIBC

TABLE A3.9: *MIBC 30ppm*

J_g, cm/s	Froth Height, cm	Weight/g	Time/s	Rate, g/s	ε_g	Pump speed	J_{wo}, cm/s
1	5				15.8776		
1.25	7				18.34187		
1.5	7	192.5	241.06	0.798556	19.74489	0.32	0.010168
1.75	7	191.5	225.34	0.849827	20.24345	0.4	0.01082
2	7	260.5	181.41	1.435974	20.40433	0.5	0.018283
2.25	7	415	225.6	1.839539	21.42135	0.54	0.023422

TABLE A3.10: *MIBC 50ppm*

J_g,cm/s	Froth Height, cm	Weight/g	Time/s	Rate, g/s	ε_g	Pump speed	J_{wo}, cm/s
1	7	494.5	300.28	1.646796	19.23902	0.5	0.020968
1.25	7	1850	300.16	6.16338	23.74546	1.1	0.078475
1.25	15	151	160.75	0.939347	23.81588	0.4	0.01196
1.5	7	4142	300.4	13.78828	26.55499	1.7	0.175558
1.5	15	1576.5	300.35	5.248876	27.22199	1	0.066831
1.5	35	400.5	300.37	1.333356	29.66529	0.44	0.016977
1.75	7	6376.5	300.62	21.21116	29.48012	3	0.270069
1.75	15	5123	300.44	17.05166	30.35191	1.96	0.217108
1.75	35	3827	300.53	12.73417	31.50927	1.62	0.162136
2	7	3800.5	180.35	21.07291	29.76298	3	0.268309
2	15	3014	180.34	16.71288	29.80184	1.92	0.212795
2	35	2823	255.41	11.05282	31.47365	1.48	0.140729

TABLE A3.11: *MIBC 80ppm*

J_g, cm/s	Froth Height, cm	Weight/g	Time/s	Rate, g/s	ε_g	Pump speed	J_{wo}, cm/s
1	7	1314	300.47	4.373149	23.55675	0.9	0.055681
1	15	189	300.66	0.628617	24.95885	0.3-0.4	0.008004
1.25	7	4105.5	300.28	13.67224	29.86287	1.7	0.17408
1.25	15	1505	370.28	4.064492	31.57161	0.84	0.051751
1.25	35	404	300.59	1.344023	33.69099	0.43	0.017113
1.25	50	249.5	300.41	0.830532	34.02922	0.3-0.34	0.010575
1.5	7	6647	300.37	22.12937	33.56772	3	0.28176
1.5	15	5211	303.03	17.19632	34.95682	2.06	0.21895
1.5	35	3203.5	300.31	10.66731	35.24753	1.44	0.13582

HEPTANOL

TABLE A3.12: *n-heptanol 30ppm*

J_g,cm/s	Froth Height, cm	Weight/g	Time/s	Rate, g/s	ε_g	Pump speed	J_{wo}
1	7	1136.5	370.25	3.069548	18.96418	0.7	0.039083
1	15	19	92.78	0.204786	21.02754	0.3-0.4	0.002607
1.25	7	2347.5	380.28	6.173083	20.34273	1.1	0.078598
1.25	15	277	315.15	0.878947	21.24284	0.4	0.011191
1.5	7	2372.5	300.71	7.889661	20.9613	1.2	0.100454
1.5	15	551	378.06	1.457441	21.36515	0.5	0.018557
1.75	7	2591.5	301.68	8.590228	22.99914	1.2-1.3	0.109374
1.75	15	541.5	300.34	1.802957	22.43664	0.54	0.022956

TABLE A3.13: *n-heptanol 50ppm*

J_g	Froth Height, cm	Weight/g	Time/s	Rate, g/s	ε_g	Pump speed	J_{wo}
0.75	7	600.5	300.46	1.998602	17.55595	0.6	0.025447
1	7	4685	375.77	12.46773	23.67375	1.66	0.158744
1	15	13.5	180.25	0.074896	25.54572	0.3	0.000954
1.25	7	7531	300.5	25.06156	30.26077	4	0.319094
1.25	15	6640	390.29	17.01299	32.44541	2.16	0.216616
1.5	7	7739.5	300.31	25.7717	29.98061	4.2	0.328136
1.5	15	7037.5	300.63	23.40917	30.73751	3.7	0.298055
1.5	35	6303	310.22	20.31784	34.46461	3.2	0.258695

TABLE A3.14 *n-heptanol 80ppm*

J_g	Height, cm	Weight	Time	Rate	ε_g	Pump	J_{wo}
0.75	7	917	300.07	3.055954	19.12983	0.7	0.03891
1	7	5103	315.71	16.16357	27.66624	2	0.205801
1	15	3288	300.41	10.94504	29.5639	1.5	0.139357
1	35	651.5	300.25	2.169858	27.60819	0.56	0.027627
1.25	7	5177	210.19	24.6301	28.75593	4.01	0.3136
1.25	15	6516	300.28	21.69975	31.7006	3.4	0.27629
1.25	35	4196	210.31	19.9515	33.18034	3.11	0.25403
1.25	50	3404	180.03	18.90796	33.39117	2.9	0.240744
1.5	7	5593	180.28	31.02396	33.76765	5.9	0.395009
1.5	15	7190	240.03	29.95459	34.18238	5.2	0.381394
1.5	35	5237	181.31	28.88423	34.58595	4.9	0.367765
1.5	50	5055	180.31	28.03505	35.18824	4.8	0.356953

OCTANOL

TABLE A3.15: *n-octanol 30ppm, 5μm sparger*

J_g	Height, cm	Weight	Time	Rate	ε_g	Pump	J_{wo}
0.75	7				14.66144	0.7	0
0.75	15				16.18777	2	0
1	7	200.5	330.25	0.607116	16.23242	0.4	0.00773
1.25	7	307.5	332.9	0.923701	17.68232	0.4	0.011761
1.5	7	453	300.22	1.508893	18.5062	0.48	0.019212
1.75	7	695	300.22	2.314969	18.95417	0.56	0.029475
2	7	996	300.22	3.317567	21.02131	0.76	0.042241

TABLE A3.16: *n-octanol 50ppm, 5μm sparger*

J_g	Height, cm	Weight	Time	Rate	ε_g	Pump	J_{wo}
1	7	4937	330.28	14.94792	22.45132	1.8	0.190323
1	15	894	180.34	4.957303	21.85891	1	0.063118
1	35	476	180.28	2.640337	21.26649	0.5-0.9	0.033618
1.25	7	5657	300.25	18.84097	22.87871	3	0.239891
1.25	15	4753	300.97	15.79227	22.84804	2.3	0.201073
1.25	35	4876.5	360.25	13.53643	23.25347	1.5	0.172351
1.5	7	4480.5	180.34	24.84474	25.48146	4.1	0.316333
1.5	15	6835	301.94	22.63695	25.85047	3.7	0.288223
1.5	35	6419.5	302.5	21.22149	26.59703	3.4	0.2702
1.75	7	5343	180.37	29.62244	28.21779	5.9	0.377165
1.75	15	5038.5	180.5	27.91413	28.41064	5.1	0.355414
1.75	35	8044	305.34	26.3444	28.74827	4.6	0.335427

TABLE A3.17: *n-octanol 80ppm,5μm sparger*

J_g	Froth Height, cm	Weight/g	Time/s	Rate, g/s	ε_g	Pump speed	J_{wo}, cm/s
0.75	7	2057	315.47	6.52043	19.84925	1.1	0.083021
0.75	15	509	180.32	2.82276	22.79566	0.7-0.8	0.03594
1	7	2945	180.25	16.33842	22.82076	2.5	0.208027
1	15	4116.5	300.31	13.7075	24.85064	1.7-1.8	0.174529
1	35	3880.5	300.18	12.92724	31	1.5-1.7	0.164595
1.25	7	4411.5	180.28	24.47027	27.44009	4	0.311565
1.25	15	7159.5	315.34	22.70407	28.27824	3.7-3.9	0.289077
1.25	35	6316.5	300.22	21.03957	28.49337	3.4	0.267884
1.5	7	5660	180.82	31.30185	31.64706	6.7	0.398547
1.5	15	5723.5	190.47	30.04935	32.20261	6.02	0.3826
1.5	35	8788.5	302.47	29.05577	32.26701	5.4	0.36995

TABLE A3.18: *n-octanol 20ppm, 20μm sparger*

J_g	Froth Height, cm	Weight/g	Time/s	Rate, g/s	ε_g	Pump speed	J_{wo}
0.5					5.711867		
0.75	0.5	1679.00	510.31	3.29016	8.152044	0.86	0.041892
1	1.5	673.5	195.38	3.45	9.826312	0.86	0.04389
1.5	3	604.5	180.12	3.36		0.86	0.042731
1.5	1.5	1180.5	180.5	6.54	12.97261	1.2	0.083272
1.75	3	613	180.4	3.40		0.86	0.043265
1.75	1.5	1374	180.35	7.62	14.74415	1.34	0.097002
2	3	790.5	225.32	3.51	16.79735	0.86	0.04467
2.5	7	632.5	180.22	3.51	19.76172	0.86	0.044686

TABLE A3.19: *n-octanol 30ppm, 20μm sparger*

J_g	Froth Height, cm	Weight/g	Time/s	Rate, g/s	ε_g	Pump speed	J_{wo}
0.75	1.5	651	180.41	3.60844743	9.4436592	0.86	0.045944
1	3	635.5	181.07	3.50969238	11.5429174	0.86	0.044687
1.5	3.5	642.5	180.09	3.56766061	15.406676	0.86	0.045425
1.75	7	525.5	180.29	2.91474846	17.5049643	0.86	0.037112
2	7	535.5	180.34	2.96939115	19.9205758	0.86	0.037807
2.5	20	530	180.41	2.9377529		0.86	0.037405
2.5	7	2050	180.43	11.3617469	22.5243652	1.72	0.144662

TABLE A3.20: *n-octanol 50ppm, 20μm sparger*

J_g	Height, cm	Weight	Time	Rate	ε_g	Pump	J_{wo}
0					5.992660736		
0.75	0.5	649.5	180.31	3.60213	9.088312656	0.86	0.045864
1	3	1085	300.09	3.615582	11.99749569	0.86	0.046035
1.5	7	614	180.38	3.403925	17.46269599	0.86	0.04334
1.75	30	815	225.31	3.617238		0.86	0.046056
1.75	7	1592	182.78	8.709924	20.30057201	1.48	0.110898
2	40	572	120.34	4.753199		0.86	0.06052
2	30	572	90.34	6.331636		1.25	0.080617
2	7	1310	100.28	13.06342	21.17277516	1.8	0.166329

ETHOXYLATED C_6 ALCOHOL

TABLE A3.21: *Ethoxy 20ppm, 5mm sparger*

J_g	Froth Height, cm	Weight/g	Time/s	Rate, g/s	ε_g	Pump speed	J_{wo}
0.75	7	133.5	380.28	0.351057	14.19621	0.4-0.3	0.00447
1	7	988	330.34	2.990858	16.44921	0.7	0.038081
1.25	7	3659	300.34	12.18286	18.5364	1.6	0.155117
1.5	7	5514.5	302.72	18.2165	22.10827	2.7	0.23194
1.5	15	104.5	150.37	0.694952	18.51326	0.4	0.008848
1.75	7	6809.5	305.94	22.25763	24.37089	3.4	0.283393
1.75	15	5216	300.16	17.3774	24.50745	2.5	0.221256
1.75	35	58.5	180.31	0.324441	26.73807	0.4	0.004131
2	7	6958	300.25	23.17402	25.3376	3.6	0.295061
2	15	4954.5	300.29	16.49905	25.32375	2	0.210072
2	35	93	300.34	0.309649	23.08543	0-0.4	0.003943

TABLE A3.22: *Ethoxy 30ppm, 5mm sparger*

J_g	Froth Height, cm	Weight/g	Time/s	Rate, g/s	ε_g	Pump speed	J_{wo}
0.75	7	975.5	331.75	2.940467	16.45029	0.7	0.037439
1	7	3029	330.85	9.155206	19.66541	1.3	0.116568
1	15	26	120.4	0.215947	18.38793	0.3	0.00275
1.25	7	5977	300.34	19.90078	25.46736	2.9	0.253385
1.25	15	5007.5	301.56	16.60532	26.19043	2	0.211425
1.25	35	4005.5	315.06	12.71345	27.73052	1.5-1.7	0.161873
1.5	7	4572	182.38	25.06854	27.21519	3.8	0.319183
1.5	15	4012	180.91	22.17677	27.92419	3.3	0.282363
1.5	35	3783.5	186.1	20.33047	28.85263	2.96	0.258856

TABLE A3.23: *Ethoxy 50ppm,5mm sparger*

J_g	Froth Height, cm	Weight/g	Time/s	Rate, g/s	ε_g	Pump speed	J_{wo}
0.75	7	901	317.16	2.840837	17.54811	0.7	0.036171
1	7	6005.5	420.25	14.2903	23.74022	1.8	0.18195
1	15	2545	300	8.483333	24.32405	1.3	0.108013
1.25	7	6657	300.43	22.15824	27.98466	3.5	0.282127
1.25	15	5912	300.87	19.64968	29.3366	3	0.250188
1.25	35	5734.5	300.19	19.1029	30.54793	2.6	0.243226
1.25	50	4983.5	300.25	16.59784	31.41749	2.1	0.21133
1.5	7	5128	180.91	28.34559	29.61105	4.9	0.360907
1.5	15	4730	180.25	26.24133	31.25161	4.4	0.334115
1.5	35	4434.5	180.63	24.55019	32.61839	4	0.312583
1.5	50	7721	340.38	22.68347	30.75423	3.6	0.288815

DOWFROTH 200

TABLE A3.24: *Dowfroth 200-50ppm*

J_g	Froth Height, cm	Weight/g	Time/s	Rate, g/s	ε_g	Pump speed	J_{wo}
1	7		179.54	0	18.47698		0
1.25	7	1048	300.34	3.489379	21.81463	0.9	0.044428
1.5	7	1862.5	300.69	6.194087	22.83934	1.2	0.078866
1.75	7	709	120.21	5.898012	22.9446	1.2	0.075096
2	7	1083	300.31	3.606274	22.60677	0.9	0.045917

TABLE A3.25: *Dowfroth 200-80ppm*

J_g	Froth Height, cm	Weight/g	Time/s	Rate, g/s	ε_g	Pump speed	J_{wo}
1	7	254	179.54	1.414727	21.93191	0.5	0.018013
1.25	7	2244	180.59	12.42594	27.39763	1.7	0.158212
1.25	15	770.5	180.25	4.274619	28.2688	1	0.054426
1.5	7	3316	180.38	18.38341	30.12356	3.1	0.234065
1.5	15	2389	180.85	13.20984	32.83511	1.76	0.168193
1.5	35	1370	180.37	7.595498	33.4999	1.3	0.096709
1.75	7	3173	180.35	17.59357	28.75566	2.9	0.224008
1.75	15	2024.5	180.44	11.2198	30.72135	1.6	0.142855
1.75	35	1302.5	180.38	7.220867	32.34279	1.2	0.091939
2	7	2596	180.28	14.39982	28.35098	2.1	0.183344
2	15	1403.5	180.69	7.767447	29.79209	1.3	0.098898
2	35	857	180.38	4.751081	30.73662	1	0.060493

TABLE A3.26: *Dowfroth 200-100ppm*

J_g	Froth Height, cm	Weight/g	Time/s	Rate, g/s	ε_g	Pump speed	J_{wo}
1	7	897.5	180.22	4.980024	22.60019	1.14	0.063408
1.25	7	2814	180.31	15.60646	28.60275	2.28	0.198708
1.25	15	1239.5	182.96	6.774705	30.11609	1.36	0.086258
1.5	7	4233.5	180.14	23.50117	33.18475	4.16	0.299226
1.5	15	3500.5	180.15	19.43103	34.85953	3.3	0.247404
1.5	35	2412.5	180.28	13.38196	35.61762	2	0.170384

DOWFROTH 250

TABLE A3.27: *Dowfroth 250-30ppm*

J_g	Froth Height, cm	Weight/g	Time/s	Rate, g/s	ε_g	Pump speed	J_{wo}
0.75	7	210	180.09	1.166084	15.31109	0.6	0.014847
1	7	1276.5	300.31	4.250608	14.5008	1	0.05412
1.25	7	2829	307	9.214984	15.88869	1.6	0.117329
1.5	7	3172	300.32	10.56207	15.75988	1.9	0.13448
1.5	15	1119	303.25	3.690025	15.16105	0.9	0.046983
1.75	7	4173	300.25	13.89842	15.9602	3.7	0.17696
1.75	15	3428	420.28	8.156467	16.85932	1.4	0.103851

TABLE A3.28: *Dowfroth 250-50ppm*

J_g	Froth Height, cm	Weight/g	Time/s	Rate, g/s	ε_g	Pump speed	J_{wo}
0.75	7	1008	306.41	3.28971	18.10326	0.9	0.041886
1	7	2897	300.25	9.648626	21.02564	1.5	0.12285
1	15	1094.5	300.06	3.647604	21.56111	0.94	0.046443
1.25	7	2800	180.06	15.55037	23.72368	2.2	0.197993
1.25	15	3558	300.85	11.82649	24.45645	1.6-1.7	0.15058
1.25	35	2275.5	304	7.485197	25.17688	1.3	0.095304
1.5	7	3380.5	180.29	18.75035	23.83063	1.9	0.238737
1.5	15	2686.5	180.06	14.92003	25.44526	1.4	0.189968
1.5	35	1943	179.97	10.79624	26.85302	1.6	0.137462
1.5	50	756	180.05	4.198834	26.82696	1	0.053461
1.75	7	3770	180.16	20.92584	25.31205	3.5	0.266436
1.75	15	2835.5	180.31	15.72569	26.10999	2.2	0.200226
1.75	35	1674	180.16	9.291741	27.02179	1.5	0.118306

TABLE A3.29: *Dowfroth 250-80ppm*

J_g	Froth Height, cm	Weight/g	Time/s	Rate, g/s	ε_g	Pump speed	J_{wo}
0.75	7	1488	240.25	6.193548	19.59322	1.2	0.078859
0.75	15	180	180.28	0.998447	21.87262	0.5	0.012713
1	7	3403	180	18.90556	27.67248	3.24	0.240713
1	15	2505.5	180.25	13.90014	28.08997	1.9	0.176982
1	35	1455.5	180.19	8.077585	27.89797	1.4	0.102847
1.25	7	5067	180.35	28.09537	31.77465	5.2	0.357721
1.25	15	4568.5	180.35	25.3313	33.43235	4.52	0.322528
1.25	35	4127.5	180.37	22.88352	35.5124	4	0.291362
1.5	7	3711	120.38	30.82738	31.53648	6.4	0.392506
1.5	15	5296	180.19	29.3912	33.93158	5.4-5.5	0.37422
1.5	35	4953	180.88	27.3828	35.31436	35	0.348649

F-150

TABLE A3.30: *F150 -30ppm*

J_g	Froth Height, cm	Weight/g	Time/s	Rate, g/s	ε_g	Pump speed	J_{wo}
1	7	1050.5	125.16	8.393257	13.88704	1.3	0.106866
1	15	893	180.32	4.952307	13.92975	0.76	0.063055
1	35	235.5	180.09	1.307679	16.09052	0.5-0.64	0.01665
1.25	7	2081	135.32	15.37836	17.30144	1.9	0.195803
1.25	15	965	120.22	8.026951	15.87813	1.3	0.102202
1.5	7	2415	120.35	20.06647	18.68514	3.44	0.255494
1.5	15	2050.5	120.5	17.0166	19.49313	2.8	0.216662
1.5	35	1574.5	120.15	13.10445	19.59332	1.76	0.166851

TABLE A3.31: *F150-50ppm*

J_g	Froth Height, cm	Weight/g	Time/s	Rate, g/s	ε_g	Pump speed	J_{wo}
1	7	1050.5	125.16	8.393257	13.88704	1.3	0.106866
1	15	893	180.32	4.952307	13.92975	0.76	0.063055
1	35	235.5	180.09	1.307679	16.09052	0.5-0.64	0.01665
1.25	7	2081	135.32	15.37836	17.30144	1.9	0.195803
1.25	15	965	120.22	8.026951	15.87813	1.3	0.102202
1.5	7	2415	120.35	20.06647	18.68514	3.44	0.255494
1.5	15	2050.5	120.5	17.0166	19.49313	2.8	0.216662
1.5	35	1574.5	120.15	13.10445	19.59332	1.76	0.166851

A3.2 BUBBLE SIZE MEASUREMENTS

TABLE A3.32: *Sauter mean diameters*

Jg	Dw250_80ppm	F150_50ppm	MIBC80ppm	Pent150ppm
0.75	0.686490478	0.71661183	0.751066704	0.7973303
1	0.788458509	0.85590049	0.874681352	0.901387182
1.25	0.956184255	1.0175093	1.138040464	1.135908427
1.5	1.30917863	1.20426574	1.497820109	1.578572532
1.75	1.508728684		1.617620394	1.684122254
2				1.8854401
2.5				2.22800922

TABLE A3.33: *d10*

Jg	Pent150ppm	MIBC80ppm	Dw250_80ppm	F150_50ppm
0.75	0.710508586	0.666713028	0.598226569	0.627506601
1	0.813488753	0.783368368	0.687480206	0.757238494
1.25	0.982946047	1.006594379	0.818071735	0.912953952
1.5	1.178943065	1.238440816	1.088429575	1.082192861
1.75	1.292759172	1.34401696	1.347443748	

TABLE A3.34: *d32*

Jg	Dw250_50ppm	F150_30ppm	MIBC30ppm	Pent100ppm
0.75	0.833946705	0.7271579	0.737992336	0.764565264
1	1.010376445	0.90189974	0.841325173	0.910715342
1.25	1.155769988	1.09204393	1.055794602	1.112033188
1.5	1.355140356	1.34799205	1.296639756	1.454602308
1.75	1.582431924	1.61435534	1.558361473	1.947405808

TABLE A3.35: *d10*

Jg	Pent100ppm	MIBC30ppm	Dw250_50ppm	F150_30ppm
0.75	0.696801336	0.668771579	0.740710354	0.639809376
1	0.801833318	0.754767977	0.915412182	0.804389569
1.25	0.931695835	0.919084021	1.032555958	0.972868508
1.5	1.077423858	1.122324748	1.223332068	1.171611688
1.75	1.390006652	1.306736043	1.450513327	1.430717798